Sudan University of Science and Technology

College of Post Graduate Studies

Charge Transfer and Separation Mechanism in Dye–Sensitized Nano solar Cells

آلية تحويل وانفصال الشحنة في الخلايا الشمسية الصبغية النانوية

Thesis submitted in fulfillment of the Requirement's for the Degree of Ph.D. in Physic's

By:

Enaam Adam Mohamed Srajalden

Supervisor:

Prof: Mubarak Dirar Abd-alla Yakhob

November 2018

الآيـــــــة

قال تعالى:((**وَلَئِنْ سَأَلْتَهُمْ مَنْ خَلَقَ السَّمَاوَاتِ وَالْأَرْضَ وَسَخَّرَ الشَّمْسَ وَالْقَمَرَ لَيَقُولُنَّ اللَّهُ ۖ فَأَنَّىٰ يُؤْفَكُونَ**))

صدق الله العظيم

سورة العنكبوت الآية

﴿٦١﴾

Dedication

I dedicate this thesis to my:

mother and father,

my dear sisters and brothers,

to my husband and my kids,

and every person who helped me to finish this work.

Acknowledgement

Firstly, I would like to thank Allah almighty for making this work possible. Secondly, I would like to express my gratitude to my supervisors Prof**.** Mubarak Dirar Abdallah, and Dr. Abdalsakhi Abdallah for his supervision, valuable advice, kind treatment and guidance during this work and to all whom support me.

ABSTRACT

Six samples of solar cells were fabrication in this research study by deposited poly (2-methoxy-5-(2'-ethyl-hexyloxy)-1.4 phenylene) (MEH-PPV) polymer layer on the indium tin oxide (ITO) glass, and deposited another layer of dye(Sodium4[2(1hydroxynaphthalen2yl)hydrazin1ylidene]7noxonaphthalene1sulfonate(EcrchromBlackT),dibenzothiatricarbocyanineIodideHexadibenzocyaini45 $C_{33}H_{29}N_2S_2I$ (DDTTC), tow samples mead by deposited zinc oxide (ZnO), cupric oxide (CuO)layers. Aluminum (Al) electrode was used to complete the formation of solar cells. The solar cells were exposed to light and the current and voltages were recorded to calculate their efficiency. The samples were characterized by Ultra violet-visible spectroscopy to display absorption spectrum. The rapid increase of the absorption in the low wavelength and decrease in special wavelength, referring to electronic transition, and this decrease is continuous with the decrease of photon energy. The range of absorption beak wavelengths for CuO +ZnO was obtained at330 nm, for MEH-PPV + DDTTC obtained at (300 nm and 500 nm) respectively.For the purpose of the present study Electronic transport in the (Six samples of solar cells) devices is studied via current density voltage (*J-V*) curves, taken using a Keithley 2400 source meter by sourcing voltage across the ITO (positive) and aluminum Al (negative)electrode .the open circuit voltage V_{oc} is the applied voltage at which the current density is zero under illumination is determined by the difference between the quasi-Fermi energy level of the (DDTTC = 2.2 eV ' Eriochrome black T = 2.16 eV ' Cu O = 2.9 eV and ZnO = 3.6 eV)and the work function of the Al electrode (4.08 eV)or the highest occupied molecular orbital (HOMO) level of the MEH-PPV in our system.

المستخلص

في هذا البحث صنعت ست عينات من الخلايا الشمسية بترسيب طبقة من البوليمر(م .إ . ه - ب . ب . ف) علي شريحة من من إول أكسيد الأنديوم تيتانيوم ورسبت طبقة اخري من الاصباغ الاتية(د .د . ت . ت .س. إ) وصبغة التفتا و عينتين رسبت فيها طبقتين من أكسيد النحاس وأكسيد الخارصين .استخدم الالمنيوم كقطب سالب للخلية الشمسية. عرضت الخلية الشمسية للضوء لدراسة خصائص الجهد والتيار وحساب الكفاءة ،و للاشعة فوق البنفسجية بواسطة جهازمطيافية الأشعة فوق البنفسجية لدراسة الامتصاصية للبوليمر والصبغات المستخدمة.حيث لوحظ زيادة سريعة في الامتصاصية عند الاطوال الموجية الصغيرة كما قلت الامتصاصية عند بعض الاطوال الموجية ،هذا يدل علي حدوث الانتقالات الالكترونية والتناقص تابع للتناقص في طاقة الفوتون.

بالنسبة للعينة (أكسيد النحاس + أكسيد الخارصين) كانت قمة الامتصاص عند الطول الموجي 330 نانوميتر اما بالنسبة للبوليمر والصبغة فكانت عند300 نانوميتر و 500 نانوميتر علي التوالي. تم دراسة منحني كثافة التيار للخلية الشمسية مع الانتقالات الالكترونية بتطبيق جهد من المصدر (كيسليي 2400) بين طرفي القطب الموجب (إول أكسيد الأنديوم تيتانيوم) والقطب السالب الألمنيوم جهد الدائرة المفتوحة هو الجهد المطبق علي الخلية عندما تكون كثافة التيار مساوية للصفر حيث يحدد بالفرق بين طاقة مستوي فيرمي(د .د . ت . ت .س إ يساوي 2.2 إلكترون فولت ، التفتا يساوي 2.16 إلكترون فولت، أكسيد النحاس 2.9 إلكترون فولت ، أكسيد الخارصين 3.6 إلكترون فولت) ودالة الشغل للالمنيوم (4.08 إلكترون فولت) او مستوي الاثارة للبوليمر.

TABLE OF CONTENTS

LIST OF TABLES

LIST OF FIGURES

Chapter One

Introduction

1.1 Solar Cells

Solar cells based on conjugated polymers are attractive due to their potential for low-cost manufacture. Power conversion efficiencies are currently approaching the values required for commercial viability, with a considerable amount of research being carried out to further improve the efficiencies [1,2]. One of the main areas highlighted for improvement is the role of charge generation and transport in such devices. The mechanism of charge generation in organic solar cells differs from that in conventional inorganic devices. In the former, light absorption results in the production of exactions, as opposed to the free electron-hole pairs which are formed in the latter [3,4]. For more efficiencies of the organic photovoltaic (OPV) response, the photo generated exactions must dissociate at the interfaces between electrons conducting and holes conducting materials. The typical diffusion length of exactions, however, is only around 20 nm [5], and thus important to maximize the interface area for a given device so as to increase the chances of exactions encountering the interface. This fact, has investigated the development of bulk hetrojunction organic solar cells containing blends of electrons and holes conducting materials, in which the fine detail of the structure creates the large interface area required [6].

Experiments performed on these so called bulk hetrojunction devices have shown that the large interface area created does indeed lead to efficient exactions dissociation, with evidence to suggest that complex composite morphologies can effect charge dissociation efficiencies [7,8]. Despite this, the overall power conversion efficiencies, while much improvements, are not as high as would be expected. This means that poor transport in the device is allowing the photo-generated charge to recombine before reaching the respective electrodes. Polymers have been used previously in photovoltaic cells, but the low electrons

mobility's of most conjugated polymers only allows them for use as the hole conducting components in a blend with other materials, such as fullerene [7], organic dyes [9] or in the present work with carbon nanotubes (CNTs). In these composite materials, the photocurrent is typically increased by several orders of magnitudes with comparison to polymer only devices.

1.2 The Importance of Research

This work deals with the transport of charges in crystalline organic semiconductors. In view of the above-mentioned "mobility puzzle" it aims at providing a deeper understanding and improved description of the relevant processes for charge transport in these materials.

1.3 The Research Problem

The research problem comes from the modeling of charge transport is essentially the modeling of the scattering of charge carriers, I have developed a transport theory based on the Holstein Hamiltonian for electron-phonon scattering. The carrier mobility is derived from a non-penrturbative evaluation of represents a generalization of the original solar cells model.

1.4 The Aim of the work

The research aims to study the Charge Transfer and Separation mechanism in dye–sensitized nano solar cells by used different dyes morphology to measure their performances and efficiency. Also to determine the influence of the transition metals and exchange layer, energy gap on the solar cell efficiency by change of electrodes material.

1.4 Thesis Layout

The thesis consists of the five chapters. Chapter one is the Introduction and Chapter two is the theoretical background about charge transport. Chapter three

the Literature Review. Chapter four consists of method and materials. Chapter five is concerned with Results, Analysis, Conclusion and Recommendations.

Chapter Tow

Charge Transport in Organic Semiconductors

2.1 Introduction

A solar cell, or photovoltaic cell, is an electrical device that converts the energy of light directly into electricity by the photovoltaic effect, which is a physical and chemical phenomenon. It is a form of photoelectric cell, defined as a device whose electrical characteristics, such as current, voltage, or resistance, vary when exposed to light. Solar cells are the building blocks of photovoltaic modules, otherwise known as solar panels. Solar cells are described as being photovoltaic irrespective of whether the source is sunlight or an artificial light. They are used as a photo detector (for example infrared detectors), detecting light or other electromagnetic radiation near the visible range, or measuring light intensity.

The operation of a photovoltaic (PV) cell requires three basic attributes:

1. The absorption of light, generating either electron-hole pairs or exactions.
2. The separation of charge carriers of opposite types.
3. The separate extraction of those carriers to an external circuit.

Charge transport in organic semiconductors is a timely subject. Today, organic semiconductors are already widely used commercially in xerography. For display and lighting applications they are employed as light emitting diodes (LEDs) or organic light emitting diodes (OLEDs) or transistors, and they are making progress to enter the solar cell market [10–11]. As a result, interest in the science behind this novel class of materials has risen sharply. The optoelectronic properties of organic semiconductors differ from that of conventional inorganic crystalline semiconductors in many aspects and the knowledge of organic

semiconductor physics is imperative to advance further with the associated semiconductor applications [12]. A central problem is the understanding of the mechanisms related to charge transport.

It may seem odd to write an article entitled "charge transport in organic semiconductors," notably polymers, when these materials are inherently insulators. This raises the question about the difference between a semiconductor and an insulator. The conductivity k of the materials is the product of the elementary charge e, the mobility μ_e of charge carriers, and their concentration n, i.e., $K^{\frac{1}{4}}$ enemies. A material can be insulating either if there are no charges available or if they are immobilized. A prototypical example of the former case is quartz. Since the absorption edge of quartz is far in the ultraviolet region (at about 120 nm), the gap E_g between the valence and conduction band is about 10 eV [13]. This implies that, at ambient temperature, the concentration of free charge carriers is practically zero. However, if one generates charge carriers by high energy radiation, they would probably move with a mobility that is comparable to that of a conventional covalently bonded inorganic semiconductor such as silicon, i.e., $1000\ \mathrm{cm^2V^{-1}s^{-1}}$ or larger. Obviously, an inherent insulator can be converted into a semiconductor if free charge carriers are generated by either injection from the electrodes, by doping, or by optical excitation. In traditional semiconductors such as silicon, germanium, or Ga_2As_3 the conductivity is between, say, 10^8 to 10^2 Ω^{-1} cm^{-1}. In un doped E_g solid, the concentration of free charge carriers is determined by($n^{\frac{1}{4}}N_{eff}e^{2/KT}$) where N_{eff} is the effective density of valence or conduction band states and E_g is the band gap. For crystalline silicon, E_g is 1.1 eV and the charge carrier mobility is about$1000\ \mathrm{cm^2V^{-1}s^{-1}}$. This predicts an intrinsic conductivity of about 10^6 Ω^{-1} cm^{-1} at room temperature. Note that a band gap of 1.1 eV translates into an absorption edge of 1,100 nm. In view of the relative dielectric constant as large

as $e^{\frac{1}{4}}$, coulomb effects between electrons and holes are un important and electrons and holes are essentially free at room temperature. This implies that optical absorption is due to a transition from the valence band to a conduction band. The situation is fundamentally different in un doped molecular solids. Their absorption edge is usually larger than 2 eV and the dielectric constant is 3-4. In this case optical absorption generates coulomb bound electron-hole pairs with a binding energy of 0.5–1.0 eV. Even if one were to ignore the exciting binding energy and to identify incorrectly the optical absorption edge with a valence to conduction band transition, the resultant intrinsic conductivity would be much less than$10^{12}\Omega^{-1}\mathrm{cm}^{-1}$, assuming a charge carrier mobility of $1\mathrm{cm}^2\mathrm{V}^{-1}\mathrm{s}^{-1}1$, i.e., the materials are insulators. However, they can become semiconducting if charge carriers are generated extrinsically.

This chapter focuses on the electronic transport of organic semiconductors. The motivation is straightforward. Modern optoelectronic devices, such as light-emitting diodes, field effect transistors, and organic solar cells are based on charge transport. The understanding of the processes that control charge transport is therefore of paramount importance for designing materials with improved structure property relations. Research into this subject was essentially stimulated by studies on charge transport in molecularly doped polymers that are now commonly used in modern photocopying machines. It turns out that xerography is mean while a mature technology [10]. It is the only technology in which organic solids are used as active elements on a large industrial scale. An important step in the historic development of xerography was the recognition that one could profitably use aromatic molecules as a photoreceptor when they are embedded in a cheap inert flexible binding material such as polycarbonates. Meanwhile, most photocopiers and laser printers use this kind of receptors although few users will recognize that once they push the print button they start an experiment on transient photoconductivity in a polymeric photoreceptor. There is much hope

that OLEDs, field effect transistors FETs, and solar cells will be able to meet the competition from existing technology based upon inorganic materials and enter the market, similarly to xerography. OLEDs that are based on small molecules already constitute a substantial business.

Apart from the endeavor to optimize the structure property relations of materials used in modern optoelectronic devices there is the desire to understand the conceptual premises of charge transport in random organic solids. The use of amorphous, instead of crystalline, organic semiconductor materials is favored because they allow for a low cost of device fabrication and the use of flexible substrates, thus enabling mechanically flexible devices. The aim of this chapter is to introduce those new to this field to the already established understanding of charge transport in organic semiconductors, and to point those familiar with the field to current research activities where new insight emerges and to the challenges that remain.

2.2 Basic working principle and efficiency

Many different designs of this general p-i-n type silicon solar cell have been developed. Single crystalline and multi-crystalline cells nowadays reach 15-20% measured solar energy conversion efficiencies. In essence silicon is not the optimal material for solar cells, its band gap of 1.1 eV (Crystalline Si) is at the lower limit for optimal solar light harvesting. The requirements for an ideal solar cell are:

Band gap between 1.1 and 1.7 eV, direct band structure Non-toxic readily available materials, easy reproducible deposition technique, suitable for large area, good photovoltaic conversion efficiency and long term stability. Silicon also suffers from its disadvantage of being an indirect semiconductor; as a result it is only a weakly absorbing material. For a silicon film to absorb 90% of the light, at least a 100 μm thick film is needed. Using direct semiconductors, like GaAs, a

1 μm thin film is sufficient. Because the photo carriers have to reach the p-n junction for separation, the silicon has to be of very high purity and crystalline perfection. For this reason the production of crystalline silicon is far from easy and cheap, and much attention is paid to the development of multi-crystalline and amorphous silicon solar cells, promising high efficiencies at lower costs. Nonetheless single crystalline silicon solar cells still have a market share of 43%, versus 48% for multi-crystalline silicon and only 8% for amorphous silicon, leaving 1% for non-silicon based solar devices [1]. A polymer solar cell has p/n transition the radiation energy of incoming sun light is directly converted into electrical energy. Polymer Solar look like photodiode with a large surface area constructed so that the Light can penetrate the p/n transition through a thin n or p conducting layer and then creates electron-hole pairs. These are separated by the intrinsic electric field in the barrier layer and can migrate in the reverse direction. Electrons migrate into the n-doped region, and the holes migrate into the p-doped region.

If the external metal contacts are shorted, short-circuit current Isc flows in the reverse direction of the photodiode. This current is substantially proportional to the number of electron-hole pairs created per unit time, i.e. it is proportional to the irradiance of the incoming light and the surface area of the solar cell. If the metal contacts are open, this reverse current leads to an open-circuit voltage V_{oc}, which in turn leads to an equal diffusion current I_D in the forward direction of the diode so that no current flows at all. If a load with an arbitrary resistance R is connected, the current I flowing through the load depends on the resultant voltage V between the metal contacts [14]. Light absorption in conjugated polymer excites electrons to a state above the low edge of the band gap but does not reach the upper edge of the band gap. This results in the formation of excitons. In this state, electrons and holes are tightly bonded by columbic attraction forces. The binding energy of excitons is 0.4 eV. These excitons can diffuse through the

polymer in the range of 10nm before vanishing. These excitons must be dissociated in order to obtain free charge carriers before they vanish. To break up the excitons, an electric field of energy greater than the binding energy of the electron hole pair require Dissociation of excitons at a hetero junction interface can generate free charge carriers. Combinations of acceptor and donor conjugated materials, conjugate material/metal layer and conjugate material/inorganic particles blend act as good interfaces for efficient dissociation of excitons due to the formation of an electron field at the junction.

2.3 Solar Cell Efficiency

There are three variables use to study the efficiency solar cell from p-n junction it conceder the basic output of the solar cell

2.3.1 Short Circuit Current (I_{sc})

The cells are characterized by many parameters, one of these parameter, is the short-current it is defined as the current that flows when the cells terminals are connected with resistant less wire. The short circuit current (Isc) that passes through the junction under elimination when the voltage is equal to zero and the maximum short circuit current that generate from the material of solar cell that join by the flux of incident photon that possess the maximum energy from energy band gap of the metal that can enable to generate the ion pairs (electron-hole) we can calculate solar cell by the silicon energy gap that equal 1.24volts as the equation

$$E_{gap} = \frac{1.24}{\lambda} \quad (2.1)$$

To find whenever the energy gap is very narrow the short current density is large because the incident photon possess enough energy to create ion pairs (electron-hole) when the energy band gap is less than its energy.

Once the light is incident to the junction of solar cell the current is from the equation

$$I = I_0\left(e^{\beta V} - 1\right) - I_P \quad (2.2)$$

Where $I_0$the saturation current, V is the voltage and I_P is the photon current.

In this case V=0 and $I = I_{sc}$ and equation (2.2) gives:

$$I_{sc} = I_o(e^0 - 1) - I_P = -I_P \quad (2.3)$$

$$I_{sc} = -I_P \quad (2.4)$$

2.3.2 Open –Circuit Voltage (V_{oc})

The other parameter is the so called open circuit voltage V_{oc} it is defined as the volt, when no current flows. It can calculate the open voltage circuit (V_{oc}) of solar cell from ideal p-n junction from the equations:

At I=0 $\quad V = V_{oc} \quad (2.5)$

$$I = I_0\left(e^{\beta V} - 1\right) - I_P$$

$$0 = I_0\left(e^{\beta V_{oc}} - 1\right) - I_P$$

$$e^{\beta V_{oc}} = \frac{I_o + I_P}{I_0} = 1 + \frac{I_P}{I_0}$$

$$V_{oc} = \frac{1}{\beta}\ln(1 + \frac{I_P}{I_0}) \quad (2.6)$$

To determinate the maximum voltage (V_{oc}) it must being I_P is very small and the acceptability estimations to minimum saturated current I_P as a function of energy gap is

$$I_P = 1.5 \times 10^5 \exp\left(\frac{-E_g}{KT}\right) A/cm \quad (2.7)$$

This relation determine the maximum value of voltage V_{oc} it decreases with decreases of energy gap this direction is the opposite case of the short circuit

current Isc and from shows there is ideal energy gap to find the maximum efficiency.

2.3.3 Fill-Factor (FF)

The short circuit current and the open circuit voltage are the maximum current and voltage respectively from a solar cell. However, at both of these operating points, the power from the solar cell is zero. The fill factor, more commonly known by its abbreviation "FF", is a parameter which, in conjunction with V_{oc} and Isc determines the maximum power from a solar cell. The FF is defined as the ratio of the maximum power from the solar cell to the product of V_{oc} and Isc graphically:

$$FF = \frac{V_m I_m}{V_{oc} I_{sc}} \tag{2.8}$$

Where FF is the fill factor.

The fill factor considers to a stander tidal referential of output characterization and its value for solar cell of the acceptable efficiency by the range between 0.7-0.85.

2.3.4 Calculation of I_{max} and V_{max}

To calculate the voltage at the maximum power V_{max} and the current at the maximum power I_{max} it can be started from equations of power:

$$P = IV = VI_0\left(e^{\beta V} - 1\right) - VI_P \tag{2.9}$$

To find $V_{max} = V_m$ at which P_{max}

$$\frac{dP}{dV} = 0 \qquad I + \frac{VdI}{dV} = 0 \tag{2.10}$$

$$I = I_0(e^{\beta v} - 1) - Ip$$

$$\frac{dI}{dV} = I_0 \beta\, e^{\beta v} \tag{2.11}$$

$$I + V_m(I_0\beta\, e^{\beta V_m}) = 0$$

$$I_0\left(\beta e^{\beta V_m}\right) - I_0 - I_P + I_0\beta V_m e^{\beta V_m} = 0$$

$$(1 + \beta V_m)e^{\beta V_m} = \frac{I_0 + I_P}{I_0} = 1 + \frac{I_P}{I_0}$$

$$\beta V_m = \ln\{(1 + \frac{I_P}{I_0})/(1 + I_0\beta V_m)\} = \ln\left(1 + \frac{I_P}{I_0}\right) - \ln(1 + \beta V_m)$$

$$V_m + \frac{1}{\beta}\ln(1 + \beta V_m) = \frac{1}{\beta}\ln\left(1 + \frac{I_P}{I_0}\right) = V_{oc}$$

$$V_m + \frac{AKT}{q}\ln\left(1 + \frac{qV_m}{AKT}\right) = V_{oc} \qquad (2.12)$$

To find $I_{max} = I_m$ at which

$$P_{max} = P = VI$$

$$\frac{dP}{dI} = 0 \qquad V + \frac{IdV}{dI} = 0$$

(2.13)

But from (2.11):

$$\frac{dV}{dI} = (\frac{dI}{dV})^{-1} = \frac{1}{\beta I_0}e^{-\beta V_m} \qquad (2.14)$$

Thus inserting (2.14) in (2.13) and substituting ($I = I_m$, $V = V_m$) yields

$$V_m + I_m\frac{1}{\beta I_0}e^{-\beta V_m} = 0$$

$$\frac{I_m}{\beta I_0}e^{-\beta V_m} = -V_m$$

$$I_m = -\beta I_0 V_m e^{-\beta V_m} = -\frac{qV_m I_0}{AKT}e^{qV_m/AKT}$$

$$I_m = -\beta I_0 V_m e^{-\beta V_m} = -\frac{qV_m I_0}{AKT}e^{qV_m/AKT}$$

$$I_{max} = I_m = -\frac{qV_m I_0}{AKT}e^{qV_m I_0/AKT} \qquad (2.15)$$

$$FF = \frac{V_{oc} - \ln(V_{oc} + 0.72)}{V_{oc} + 1}$$

And by knowing the three parameters we can calculate the solar cells efficiency [15]

$$\eta = \frac{V_m I_m}{P_{in}} = \frac{V_{oc} I_{sc}}{P_{in}}$$

2.4 Basic Concepts of Charge Transport in Organic Solids

There are many concepts of Charge Transport in Organic Solids must be understanding.

2.4.1 Electronic Structure of Organic Solids

In order to understand charge transport in organic solids, we need to elaborate on the electronic structure of organic solids. Organic solids such as molecular crystals, amorphous molecular films, or polymeric films are made of molecular subunits. We shall therefore start from a molecular picture and consider any coupling between the molecular units afterwards. Organic semiconductors are hydrocarbon molecules with a backbone of carbon atoms. The strong bonds that form the molecular backbone arise from sp^2 hybridized atomic orbitals of adjacent carbon atoms that overlap yielding a bonding and anti-bonding molecular s and s^* orbitals. The remaining atomic P_z orbitals overlap to a lesser degree, so that the resulting molecular p and p^* orbitals are less binding or anti-binding, thus forming the frontier orbitals of the molecule. In the ground state of the molecule, all bonding orbitals up to the highest occupied molecular orbital, the HOMO, are filled with two electrons of antiparallel spin while the anti-bonding orbital's, from the lowest unoccupied molecular orbital (LUMO) onwards, are empty. Neutral excited states can be formed for example by light absorption in a molecule, when an electron is promoted from the HOMO to the LUMO. In general, any configuration with an additional electron in an anti-bonding orbital and a missing

electron in a bonding orbital, i.e., a hole, corresponds to a neutral excited state. Due to the low relative dielectric constant in organic semiconductors (on the order of 3 eV), coulomb attraction between electron and hole is strong, resulting in an exciting binding energy ranging from of 0.5 eV to more than 1 eV. Molecular orbital diagrams corresponding to the configurations in the ground or neutral excited states are shown in Fig (2.1). For charge transport in organic solids to take place, there must be a charge on the molecular unit. This may either be an additional electron that is accommodated in an anti-bonding orbital, or one that is removed from a bonding orbital. The molecule is then no longer in the ground state but rather in a charged excited state. The addition or removal of an electron from the molecule may be obtained in several ways:

1-Through injection or extraction of an electron at the interface between a metal electrode and the molecule, as is typically the case in the operation of a device such as light-emitting diodes (LED).

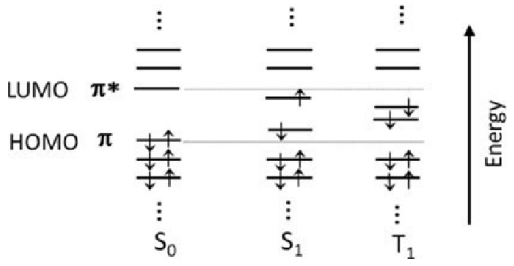

Figure (2.1) Molecular orbital diagram showing the electronic configuration for the ground state (S_0), for the first spin-singlet excited state (S_1) and for the first spin-triplet excited state (T_1).

2-through exothermic dissociation of a neutral excited state in molecule by electron transfer to an adjacent molecule. This process leads to the generation of geminately bound electron-hole pairs as precursors of free positive and negative charges in an organic solar cell. From electrochemical experiments it is well known that, after the removal of one electron from an individual molecule, more energy is required to remove a second electron. This implies that the relative

positions of the molecular orbitals with respect to the vacuum level change upon removal or addition of an electron, as indicated in Fig. 2a in a qualitative fashion. Furthermore, when an electron is taken from a p-orbital or added to a p* orbital, this alters the spatial distribution of electrons in the more strongly bound s-orbitals, resulting in different bond lengths of the molecule. The energy associated with this change in molecular geometry is known as the geometric reorganization energy, and the charge in combination with the geometric distortion of the molecule is referred to as a polar on. These effects due to electron–electron correlations and electron–phonon couplings are a manifestation of the low dielectric constant of organic semiconductors. They are absent in inorganic semiconductor crystals due to the strong dielectric screening with (e). A charged molecule may absorb light in the same fashion as does a neutral molecule, thereby promoting an electron from a lower to a higher molecular orbital. Possible optical transitions are indicated in Fig (2.2) by arrows. These optical transitions can easily be observed in doped molecular films as well as in solution (see below). We note that, analogous to transitions in neutral molecules, Absorption.

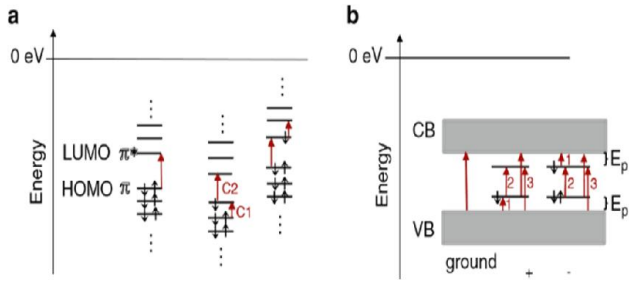

Figure (2.2) (a) Molecular orbital diagram for a neutral molecule in the ground state for a positively charged molecule, and for a negatively charged molecule. (b) Semiconductor band picture showing self-localized polar on energy levels within the band gap.

When molecules are not in a gas phase but in a solid, the absolute values of their energy levels shift with respect to the vacuum level due to the change in the

polarization of their surroundings. If they are deposited, by spin-coating or evaporation, to form an amorphous film, the surrounding polarization varies spatially in a random fashion leading to a random distribution of the absolute values of the molecular energies. By the central limit theorem of statistics, this implies a Gaussian distribution of excited state energies [16] for both neutral and charged excited states, with a variance (s) that is characteristic for the energetic disorder. Experimentally, this is observed as an inhomogeneous broadening of the optical spectra such as absorption, fluorescence, and phosphorescence spectra. Hole and electron transporting states are similarly disorder broadened although in this case state broadening is not directly amenable to direct absorption spectroscopy. Such disorder is absent in a molecular crystal. In an inorganic semiconductor crystal, such as Si or Ge, atoms are bound by strong covalent bonds to form the crystal. Consequently, electronic interactions between the atomic orbitals are strong, and wide bands with bandwidths on the order of a few eV are formed that allow for charge transfer at high mobility. In contrast, molecular crystals are kept together by weak van der Waals bonds. Consequently, electronic interactions between the molecular orbitals of adjacent lattice sites are weak and the resulting bands are narrow, with bandwidth below 500 meV [17]. In very pure molecular crystals of, say, naphthalene or beryline, band transport can therefore be observed from low temperatures up to room temperature [18–19]. At higher temperatures, intra- and intermolecular vibrations destroy the coherence between adjacent sites. A charge carrier is then scattered with a mean free path that approaches the distance between adjacent sites. As a result, band transport is no longer possible and charge carriers move by hopping .On passing, we note that even though charge transport in pure molecular crystals takes place in a band, optical transitions in a molecular crystal do not take place between valence and conduction bands due to a lack of oscillator strength. This is an inherent consequence of the strong coulomb interaction present between charges in molecular crystals. While in inorganic crystals, the strong dielectric constant

implies an effective shielding of coulomb forces, this is not the case in organic crystals due to their low dielectric constant. It implies that when an optical transition is to take place, in order for an electron to escape from its coulombically bound sibling, it had to overcome a coulomb capture radius which is about 20 nm. The electronic coupling among molecules that far apart is negligibly small, resulting in negligible oscillator strength for such a "long distance charge-transfer type" transition. Therefore, a transition such that the electron is outside the coulomb capture radius of its sibling does not take place. Rather, absorption and emission in a crystal takes place between orbitals of an individual molecule on a particular lattice site, or between orbitals of immediately adjacent molecules, thus yielding strongly coulombically bound electron hole pairs, referred to as Frenkel exciting or charge transfer exciting, respectively. In a perfectly ordered crystal, the exciting, i.e., the two-particle excitation is equally likely to be on any lattice site and thus couples electronically to neighboring sites. This results in the formation of an exciting band, i.e., a band for the two-particle excitation, within which the exciting moves in a delocalized fashion. Note that the exciting band describes the electronic coupling between an existing two-particle excitation on a molecule with its neighboring site (and thus the motion of an exciting), while the p or p* bands describe the coupling of a one-particle molecular orbital with its neighbor. p or p* bands are therefore suitable to portray the motion of a single charge carrier in a molecular crystal, yet, for the reasons just outlined, optical transitions between them do not occur.

Today's organic semiconductor devices such as LEDs, FETs, or solar cells may be made from amorphous molecular films, molecular crystals (in the case of some FETs), or from polymeric semiconductors. In polymers, molecular repeat units are coupled by covalent bonds allowing for electronic interaction between adjacent repeat units. As will be detailed in the next section, in a perfectly ordered polymer, such as crystalline polydiacetylene [20], this electronic interaction leads

to the formation of a broad intra-chain exciting band as well as valence and conduction bands while inter-chain interactions are moderately weak and comparable with the situation of molecular crystals. In amorphous polymers, conformational disorder implies that coherence is only maintained over a few repeat units that thus form a chromophore [21]. We refer to this section of the polymer chain as the conjugation length. Naturally, the conjugation length in rigid, well ordered polymers such as MeLPPP is longer (on the range of 10–15 repeat units) than in polymers with a high degree of torsional disorder along the chain such as DOO-PPP [22, 23]. A charge carrier on a polymer chain may move coherently within the conjugation length, though hopping will take place between different conjugated segments [24, 25]. For the purpose of considering charge transport, it is therefore convenient to treat a conjugated segment of a polymer chain as a chromophore, i.e., analogous to a molecule.

So far we have outlined the conceptual framework in which we discuss charge transfer in organic semiconductors. It is based on a molecular picture where the molecular unit is considered central, with interactions between molecular units added afterwards. For amorphous molecular solids and for molecular crystals this approach is undisputed. In the case of semiconducting polymers, a conceptually different view has been proposed that starts from a one-dimensional (1D) semiconductor band picture, and that is generally known as the Su–Schrieffer–Heeger (SSH) model [26–27].

We feel the molecular approach we have taken gives an appropriate description of the underlying electronic structure. The conceptual framework one adopts however influences the interpretation of experimental results, for example when considering the absorption spectra of charge carriers. In order to place the discussion of charge transfer models for polymers into a larger context, it is beneficial to be aware of agreements and differences between a “molecular

approach" and the SSH model. Therefore we shall digress here to a comparative discussion of the two approaches.

2.4.2 Transport at Low Carrier Density

The mobility of charge carrier is a key parameter for the understanding of electronic phenomena in organic semiconductors used, for instance, in electrophotography, and in modern devices such as organic light emitting diodes (OLEDs), field effect transistors (FETs), and photovoltaic (PV) cells. It determines both the device current and, concomitantly, the device efficiency as well as its response time. Devices of practical use are often layers of molecularly doped polymers, vapor deposited p-bonded oligomeric molecules, or p conjugated main chain polymers. In such systems, disorder is a major issue for the structure–property relation. Since there is already a wealth of understanding of salient disorder phenomena pertinent to charge transport in such systems [21], we shall only summarize earlier achievements and concentrate in more detail on more recent developments instead.

2.4.3 Coherent Band Transport

I proceed in order to extract the essential physics and discuss Equation. of the carrier mobility in terms of contributing scattering events. This is most intuitive if the zeroth order of electron-phonon inter action ($G^Q = 0$) is split off in the third line Eq. of the carrier mobility:

$$e^{-\sum Q^{\phi} Q(t) G_0^Q L_0 N e^{-iQR_M}} = 1 + (e^{-\sum Q^{\phi} Q(t) G_0^Q L_0 N e^{-iQR_M}} - 1) \qquad (2.16)$$

In terms of physics, I separate coherent transport (no phonon-scattering) from incoherent transport (scattering by phonons). Accordingly, one obtains

$$\mu_{\alpha\beta} = \mu_{\alpha\beta}^{coh} + \mu_{\alpha\beta}^{inc} \qquad (2.17)$$

Where the coherent part reads

$$\mu_{\alpha\beta}^{coh} = -\frac{e_0}{2N_C K_B T \hbar^2} \sum_{LMN} R_{L\alpha} \varepsilon_L R_{N\beta} \varepsilon_L \times \frac{1}{N_\Omega} \sum_{K_1 K_2} e^{-iK_1(R_M+R_N)} e^{iK_2(R_M-R_N)} \times$$

$$n_{k1}(1-n_{k2}) \int_{-\infty}^{\infty} dt\, e^{\frac{it}{\hbar}[\varepsilon(k1)-\varepsilon(k2)]} \qquad (2.18)$$

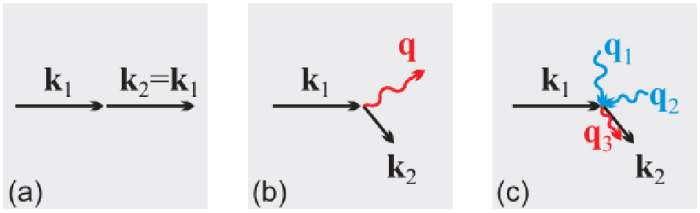

Figure (2.3): Typical coherent (a) and incoherent (b) and (c) processes involved in carrier transport. In (c) a third order process (one emitted and tow absorbed phonons) with resulting phonon wave vector $q=q_1+q_2-q_3$ is displayed

This mobility expression can be interpreted in terms of contributing scattering events from some initial states k_1 into final statesk_2. The sum over k_1 and k_2 in (2.18) includes all such events according to the probability n_{k1} that an initial state is occupied times the probability $(1-n_{k2})$ of the final state being empty (Pauli blocking factor). From the time integration in Equ.(2.18) it gets obvious that the energy of the initial polaron $\mathcal{E}(K_1)$ has to match the energy of the final polaron $\mathcal{E}(K_2)$ (energy conservation). Moreover, considering the real space sum over the index M which only occurs in the exponentials gives a Kronecker delta in the wave vectors of initial and scattered polaron $\delta\, k_1,k_2$ (momentum conservation). Such a (maybe trivial) scattering event, where initial and final wave vectors coincide is depicted in Fig. (2.3) (a). The momentum conservation in the polaron wave vectors in $\mu^{(coh)}$ reflects the coherence aspect of band transport, i.e., the moving particle does not lose its phase coherence and its momentum relaxation length is infinite. From the momentum conservation it follows that $\mathcal{E}(k_1)=\mathcal{E}(k_2)$ is immediately fulfilled and one observes that the mobility $\mu^{(coh)}$ becomes infinite, as expected for coherent transport without any scattering mechanism. In real crystals, the mean free path (or the coherence time) can be reduced by other

scattering mechanism beyond the model (impurities, disorder, electron-electron scattering ...). Such processes may be accounted for by the introduction of a disorder parameter τ similarly to previous work. Therefore, I introduce a constant limiting scattering time and replace technically

$$\int dt \rightarrow \int e^{-(\frac{t}{\tau})^2} dt \tag{2.19}$$

More complicated expressions for the scattering time such as a k dependent form are avoided here since these scattering mechanisms are not in the focus of the present work. The Gaussian broadening limits the coherence time to τ. The corresponding energy ħ/τ can be regarded as a static disorder parameter which mimics different on-site energies for example.

The resulting mobility can be written as

$$\mu_{\alpha\beta}^{\mathrm{coh}} = \frac{\sqrt{\pi}\mathrm{e}_0\tau}{2\mathrm{N_C}\mathrm{K_B}\mathrm{T}} \sum_{\mathrm{K}_1} \mathrm{n}_{\mathrm{k}1} \, (1 - n_{k1}) v_\alpha(k_1) v_\beta(k_1) \tag{2.20}$$

Where I have introduced the polaron band velocity

$$v_\alpha(k) = \frac{1}{\hbar} \frac{\delta\varepsilon(k)}{\delta k_\alpha} \tag{2.21}$$

The fact that the band velocity appears explicitly in Equ. (2.20) is a result of the underlying coherence character of this transport contribution. The tilde in (2.21) is reminiscence to its polaronic nature and therefore temperature dependence because it is affected by the band narrowing.

Apart from the tildes, Equ. (2.20) is a well-known expression that may also be derived from the Boltzmann transport equation. However, an essential difference is that the expression (2.20) is now generalized to polarons. The limit of small electron-phonon coupling is discussed, where the polarons reduce to the bare particles and the expression from the Boltzmann equation is recovered. Finally, I give another form of the result for the coherent part of the mobility. If the squared

velocity $v_\alpha^2(k)$ is written as $v_\alpha^2(k)\varepsilon(k)$ one can further introduce the polaron density of states:

$$D(\varepsilon) = \sum_k \delta[\varepsilon - \varepsilon(k)] \tag{2.22}$$

And write the diagonal elements of the mobility tensor as

$$\mu_\alpha^{coh} = \frac{\sqrt{\pi} e_0 \tau}{2 N_C K_B T} \int_0^\infty d\varepsilon \, D(\varepsilon) \, n_\varepsilon (1 - n_\varepsilon) v_\alpha^2(\varepsilon) \tag{2.23}$$

Again, Equ. (2.23) is also similar to a well-known textbook formula with the generalization of all quantities (DOS, energy, occupation, velocity) from electrons to polarons [28].

Chapter Three

Literature Review

3.1 Introduction

The mechanism of charge generation in organic solar cells differs from that in conventional inorganic devices. In the former, light absorption results in the production of exactions, as opposed to the free electron-hole pairs [29, 30]. For more efficiencies of the organic photovoltaic (OPV) response, the photo generated exactions must dissociate at the interfaces between electrons conducting and holes conducting materials. The typical diffusion length of exactions, however, is only around 20 nm [31], and thus important to maximize the interface area for a given device so as to increase the chances of exactions encountering the interface. This fact, has investigated the development of bulk heterojunction organic solar cells containing blends of electrons and holes conducting materials, in which the fine detail of the structure creates the large interface area required [32].Experiments performed on these so called bulk heterojunction devices have shown that the large interface area created does indeed lead to efficient exactions dissociation, with evidence to suggest that complex composite morphologies can effect charge dissociation efficiencies [33,34]. Despite this, the overall power conversion efficiencies, while much improvements, are not as high as would be expected. This means that poor transport in the device is allowing the photo-generated charge to recombine before reaching the respective electrodes. Polymers have been used previously in photovoltaic cells, but the low electrons mobility's of most conjugated polymers only allows them for use as the hole conducting components in a blend with other materials, such as fullerene [33], organic dyes [35] or in the present work with carbon nanotubes (CNTs). In these composite materials, the photocurrent is

typically increased by several orders of magnitudes with comparisons to polymer only devices.

3.2 Utilizing Carbon Nanotubes in Organic Solar Cells

Charge transport in carbon nanotubes-polymer composite photovoltaic cells transport has been done by Adnen Ltaief. Experimental Section the MEH-PPV conjugated polymer and the SWNTs (Carbolex AP-grade, 12-15 angstrom diameter) were purchased from Aldrich. MEH-PPV has a molar mass of 86 000 g/mol determined by gel permeation chromatography (GPC). The ITO substrates were cleaned in an ultrasonic bath of acetone (HPLC grade) for 20 min, followed by isopropyl alcohol (IPA, HPLC grade) rinsing for 20 min at room temperature, before being dried in nitrogen gas flow. MEH-PPV: SWNTs (1:1) composite solutions were prepared by blending the MEH-PPV with the SWNTs in an appropriate solvent, at a concentration of 15 mg/mL, and dispersing the SWNTs by using a magnetic stirrer. Sonication for 30 min is sufficient to give a stable transparent solution. In the first part of this work, the organic active layer of MEH-PPV or MEH-PPV: SWNTs (1:1) composite, is sandwiched between two electrodes on a glass substrate. The bottom electrode is an ITO layer, which serves as the anode and the top electrode is an Al layer, which is used as the cathode. In forward bias condition, the positive voltage was applied to the ITO layer with respect to the metal electrode. Photovoltaic cells were fabricated by spin coating (2,000 rpm for 20 s) the active bulk heterojunction layer onto a 100 nm precleaned ITO glasses of 1 cm × 1 cm coated with PEDFOT: PSS layer, using a “P6700 Series” spin coater. A layer of PEDOT: PSS between the transparent ITO electrode and the photoactive layer has been deposited from an aqueous solution onto the ITO substrate with an angular speed of 1,500 rpm. PEDOT: PSS films were dried on a hot plate under a nitrogen atmosphere for 10 min at 120 °C. Completion of the photovoltaic device occurs when aluminum contacts (typical thickness ~ 170 Å) are applied to the MEH-PPV: SWNTs

composite film layers. This is accomplished using thermal evaporation under vacuum at pressures <10-6 mbar with a standard shadow mask. The approximately thickness of the polymer/SWNTs layers was of the order of 500 nm. The effective solar cell area as defined by the geometrical overlap between the bottom ITO electrode and the top cathode was 0.1 cm2. The short circuit current and I-V curves were measured using a "Keithley 6430 SUB-FEMTOAMP REMOTE Source meter" source unit, using a Halogen lamp for illumination. Photovoltaic cell testing was performed in an isolated black box configuration to assure standard calibration and reproducibility of results. All processing steps were carried out in clean room conditions [36].

Adnen Ltaief has investigated the effect of SWNTs doping on the charge transport mechanisms of MEHPPV and MEH-PPV: SWNT (1:1) devices. Hopping of carriers between localized electronic states of the MEH-PPV polymer constitute the main mechanism for carrier transport. A clear link between the exponential distribution of the localized states and the observed power-law behavior of the only MEH-PPV device has been identified. The observed space-charge limited current (SCLC) regime of the photovoltaic cells is explained by an exponential tail state model for the polymer matrix, which is modified by the embedded SWNTs. The ability to construct organic D/A network composite photovoltaic cells containing single-walled carbon nanotubes (SWNTs)-polymer (MEH-PPV) composites has been demonstrated. The relatively high values of series and shunt resistances can be explained by a reduced photo generation rate and increased recombination rate, which is exacerbated by the proportional metallic nanotubes in the composite layers.

Also Richard Elkins utilizing carbon nanotubes to improve efficiency of organic solar cells. He used multi-walled carbon nanotubes as the electron donor and MEH-PPV-CN as electron acceptor. The CNTs were supplied and their diameter

was 5-15 nm, their length was 0.5-5 μm, and were 60% metallic and 40% semiconducting. The CNTs were functionalized to improve their solubility.

Richard Elkins modeling the theoretical design standpoint for broke the current generation process down into four phases: photo generation of exactions, excitonic transport to the junctions, electron-hole separation, and charge transport to the electrode. The team looked at each of these steps from a conceptual and mathematical perspective and worked to develop a strong understanding of what steps (i.e. device thickness, material location/structure/concentration) he would take to optimize the device's output. It may turn out that one process is much slower than the others and the model for that "rate limiting step" becomes more important than the rest. However, He does not know if this is the case. In general, modeling bulk hetrojunction organic solar cells requires the use of extremely complex mathematical treatments that extend well beyond the capabilities of a one semester senior design project. His approach to the problem must be simplified to focus on understanding the physics of polymer/nanotube solar cells on a basic level and applying this knowledge to our design. He will begin with a preliminary model of a simple bilayer hetrojunction, for which models can be developed, and he shall extend the relevant results towards understanding the bulk hetrojunction [37].

The design of these components came from background knowledge that he spent a considerable amount of time collecting. Previous literature on the topic of organic solar cells provided helpful information and directions for our project.He looked to extend the well-studied trend of using C60 "Bucky" balls in the polymer to using carbon nanotubes. He developed a basic model that he felt should produce the best possible efficiency if we were able to place the materials in exact locations within the device. This model is simply a theoretical proposal; there is still work to be done mathematically and experimentally to verify if even his basic modeling assumptions was accurate. While he was designing an essentially

optimal device, he was also working to create an operational device in the lab. Many devices were created using everything from pure polymer to pure nanotubes and many mixtures of the materials. While he was unable to produce a non-shorting device he feels reducing the concentration of nanotubes and restricting nanotube agglomeration will lead to fewer shorts. Overall, he was able to theoretically design a device, apply some of his theories within the lab, develop a recipe for fabrication, characterize a series of devices, and develop some theories for how he could improve the process in the future.

Also performance improvement of MEH-PPV: PCBM solar cells using bathocuproine and bathophenanthroline as the buffer layers was done by L.X. Dphg all the devices in this work were fabricated on indium tin oxide (ITO)-coated glass substrates, which had been carefully cleaned by acetone, ethanol and de-ionized water consecutively, and finally dried by blowing with nitrogen gas and baking at 80 ◦C for 5 min in air. After the dried ITO glass substrates was treated by UV ozone for 10 min, the filtered poly(3,4-ethylenedioxythiophene):poly(styrenesulfonate)(PEDOT:PSS) was spin coated on the top of the ITO surface with a speed of 2000 rpm (round per minute) for 50 s and then annealed in a vacuum at 120 ◦C for 10 min. The MEH-PPV: PCBM, dissolved in chlorobenzene with a weight ratio of 1:4, was spin coated onto the PEDOT: PSS layer at the same speed of 2000 rpm. Layers of Bphen, BCP, LiF and an aluminum (Al) electrode were thermally evaporated under high vacuum. Deposition rates were monitored with a quartz oscillating crystal and controlled to be 1 ˚A/s for both organic layers and LiF. A shadow mask was used for the deposition of the cathode, giving an active device area of 0.1 cm^2. The device configuration of organic photovoltaic cells used in the study.

He was investigated the effects of interfacial buffer layers—BCP and Bphen on the performance of polymer solar cells based on MEH-PPV and PCBM blend. After inserting 5-nm BCP and 12-nm Bphen between the active layer and the

cathode, the PCE are substantially increased by a factor of 0.69 and 1.16, respectively, as compared with the devices without any buffer layer. The roles of BCP and Bphen might be the same for efficiency improvement because of their similar optical transparency and energy gap. How- ever, compared with traditional devices by using LiF as the buffer layer, the BCP-based devices show a com- parable efficiency, while Bphen-based devices show a much higher efficiency. This is due to the better electron transport ability of Bphen than that of BCP [38].

Also non-linear I–V characteristics of MEH-PPV patterned on sub-micrometer electrodes was done by J.H. Parka, the heavily doped Si substrate was thermally oxidized and was spin-coated by an e-beam resistor ŽPMMA. On the oxidized substrate. He drew the electrode pattern directly using an e-beam lithography ma- chine. After development, a negative PMMA pattern remained. A NiCr alloy was deposited to improve adhesion to the substrate before a thick Pt layer was deposited, which was evaporated by e-gun. At the lift-off process, we removed all of the negative PMMA pattern in the acetone. In this way, a Pt electrode on the oxidized substrate was fabricated. MEH-PPV dissolved in p-xylene was spin- coated onto the Pt electrode. He drew the e-beam line across the Pt electrode using a SEM. The solubility of the polymer was affected by the high energy electrons. The polymer was developed in p-xylene to dissolve unexposed polymer. The MEH-PPV patterned electrode was attached to a chip carrier by silver paste. The electrode and external probes were connected by wire bonder. The sub- micrometer-sized device of the un doped polymeric semiconductor was measured at various temperatures using a cryostat in a vacuum. Constant voltage was supplied by Keithley 6517A and the resulting current was measured by another Keithley 6517A. The noise level during the I–V measurements was a few pA while the signal level was nA. Because the resistivity of the sample was so high

and the RC response time was so long, we took the data after the signal was stabilized.

This method of mask less patterning to make a sub- micrometer-wide line of conjugated polymer MEH-PPV was done using SEM. The I–V characteristics of the patterned MEH-PPV line were measured as a function of temperature. Non-linear I–V curves were fitted in the high field region using a single carrier [39].

3.3 Optical and Electrical Characteristics of Organic Solar Cells

The change of energy gap and efficiency of carbon solar cell when doped by some elements was done by Mubarak Dirar Abdalla,to study the change of energy gap and efficiency of carbon solar cell when doped by some elements. He used six samples which prepared where C is doped with Zn, Mg, Al, S, Cd and Cu. The absorption, energy gap. When the carbon solar cell was doped with Mg, Al, S, Cu, Zn and Cd, the energy gap and efficiency changes. For Mg, Al, S, and Zn with atomic numbers Z: 12, 13, 16, and 30, the energy gap E_g increases and takes values 1.879, 1.897, 1.918, 1.925 eV respectively. This may be related to the fact that, according to hydrogen like atoms, the energy gap increases with atomic number. However the efficiency decreases for this group to be 0.780, 0.730, and 0.023 for Al, S, and Zn respectively. This is since the increase of energy gap decreases the number of electron that reaches conduction band, which in turn decreases efficiency. For Cu and Cd with Z= 29 and 48 Eg decreases to be 5.184 and5.107 respectively. This is related to the inverse effect of atomic radius on, where r increases with Z. The efficiency increases as E_g decreases.

The results show that the efficiency and energy gap of carbon solar cell is affected by the atomic number. This raises a hope in increasing efficiency by doping solar cells with impurities [40**]**.

Also determination of energy Gaps and effect of temperature on the absorption and transmittance spectrum on photoelectrodye was done by Asim Ahmed

Mohamed Fadoll, is concerned with determination of energy gaps and effect of temperature on the absorption and transmittance spectrum on photoelectron dye. In this work a sample of fresh Roselle was making .The optical properties of the dye Roselle anthocyanin's shows high absorption to visible spectrum because of concentration of anthocyanin in Roselle calyces. Its absorption to sun light is almost constant which an indication of chemical stability. The absorption spectrum of the anthocyanin dye dissolved in methanol shows λ_{max} v(283 nm) in the UV region, while λ_{max} (545 nm) in the VIS range. The corresponding energy levels are 4.36 eV and 2.25 respectively .The absorption spectrum of fresh Roselle crude shows in the visible region. The energy gap of Roselle is 2.06, while that of titanium dioxide is 4.125. These values agree with the standard values. The response of optical absorption to temperature shows stability at ambient temperature, while absorption decreases as temperature increases above ambient temperature.

The results obtained show that the thermal properties of the Roselle anthocyanin dye indicates that its absorption property, i.e., the ability of atoms to trap visible photons, is stable and does not affected by temperature at ordinary ambient temperature. But at higher temperatures the absorption decreases. It shows also almost temperature absorption to direct sun light thus indicates high chemical stability. The optical property of the Roselle anthocyanin dye shows high efficiency to absorb visible light. This may have a direct impact on increasing the efficiency of the solar cell, as for as the function of the dyes to trap visible light [41].

Also optical properties of glass and plastic doped by CU was done by Elharam Ali Eltahir Mohammed, Five samples plastics and glasses were doped by Cu with different concentration ranging from 28.9 $\boldsymbol{\mu}$g/cm2 to 1965.8$\boldsymbol{\mu}$g/cm2. The optical properties of samples were studied by using the following devices with the following specification. Glass and plastic samples are doped with Cu at different

concentrations. The results obtained show that increasing Cu concentration decreases absorption coefficient, refractive index, real and imaginary electric permittivity, whereas energy gap increases. These results surprisingly agree with the theoretical model that treats Cu as an electric dipole.

The results show that absorption of light by glass can be changed by changing the concentration of Cu. The increase of Cu concentration decrease absorption coefficient. This means that in the design of windows in homes one can enable more light to pass into the room, by decreasing concentration of Cu. It can be also be used in designing sensor and solar cells to improve their performance [42].

Also optical and electrical characteristics of TIO2 – MEH multilayers thin film was done by Tayiser MohiEldin Elmahdi, The organic compounds MEH-PPV and TiO2 was used in this study to construct four samples which are multi-layers structures to study their optical and electrical characteristics.

The optical and electrical properties of TiO2-MEH-PPV double layer was studied when their number is increased. It was found that increasing the number of double layers decreases the energy gap which may result from the effect of the internal MEH electric field that allows some energy levels to enter the energy gap. The absorption also increases when layers were increased which may result from the narrowing of the energy gap. The current however decreases up on increasing the layers which may be related to the increase of electric resistance.

The results show that the energy gap of TiO2 - MEH double layer can be decreased and the absorption can be increased by increasing the number of them. Thus increase of TiO2 - MEH layers decreases current [43].

Also energy gaps, donor and accepter levels for polymer solar cells doped with different dyes was done by Enam Izeldin Ibrahim Elsayd. The energy levels and energy gaps of polymer solar cells values were found when they are doped with Coumarin, Lawsonia, Rohdamin B, Blue 8GX, Roselle, DDTTC and Ero-Chrom

black, by means of the values of absorption and transmission spectra, beside values of absorption coefficient- intensity relations of them. The results obtained for shows that the absorption spectra which relates intensity and emitted wave lengths for them gives the values of donor and acceptor levels which are 5.07 , 4.41 , 5.08, 5.12 ,4.57, 4.88, 5.54eV respectively 2.43, 2.25, 2.45, 2.84, 2.32 , 2.41 2.33eV respectively. The transmission spectra for Coumarin, Lawsonia, Rohdamin B, Blue 8GX, Roselle, DDTTC and Ero-Chrom black is closely related to their energy gaps which were found to be 1.17, 3.58, 1.10, 1.08, 3.06, 1.52, 1.11 eV these values are in conformity with the results obtained by the absorption coefficient - intensity relations which predicts the energy gaps 3.55, 3.30, 3.27, 3.15, 3.08, 2.94eV and 2.59eV which are in agreement with the standard values.

The results show that the application of conducting polymers to optoelectronic devices such as solar cell. Dyes Structure showed high optical absorption in the range of (200 to 537) nm. To increase power conversion efficiency, structures of the solar cells should be optimized [44].

Also comparison of transparent conductive indium tin oxide, titanium-doped indium oxide, and fluorine-doped tin oxide films for dye-sensitized solar cell application was done by Dong-Joo Kwak, the TCO materials investigated in this study are ITiO, ITO, and FTO. The FTO glass is commercially available from Pilkington Co., whereas the thin films of ITiO and ITO are prepared using RF magnetron sputtering. In this study, He investigate the photovoltaic performance of transparent conductive indium tin oxide (ITO), titanium-doped indium oxide (ITiO), and fluorine-doped tin oxide (FTO) films. ITO and ITiO films are prepared by radio frequency magnetron sputtering on soda-lime glass substrate at 300 °C, and the FTO film used is a commercial product. He measure the X-ray diffraction patterns, AFM micrographs, transmittance, and sheet resistances after heat treatment, and transparent conductive characteristics of each film. The value of electrical resistivity and optical transmittance of the ITiO films was 4.15×10-

4 Ω-cm. The near-infrared ray transmittance of ITiO is the highest for wave lengths over 1,000 nm, which can increase dye sensitization compared to ITO and FTO. The photo conversion efficiency (η) of the dye-sensitized solar cell (DSC) sample using ITiO was 5.64%, whereas it was 2.73% and 6.47% for DSC samples with ITO and FTO, respectively, both at 100mW/cm^2 light intensity.

In this study, He investigate the photovoltaic performance of transparent conductive ITiO, FTO, and ITO thin films. ITiO and ITO thin films are deposited on a soda-lime glass substrate by RF magnetron sputter method at relatively low substrate temperature (~300 °C) and at high rate (~10 nm/minutes), whereas the FTO film used is a commercial FTO glass. He investigate the electrical and optical properties of these films such as X-ray diffraction patterns, AFM micrographs, optical transmittance, sheet resistances, and photovoltaic characteristics. The near-IR transmittance of ITiO is the highest for wavelengths over1,000 nm, which can increase dye sensitization in DSCs compared to ITO and FTO. The photo conversion efficiency (η) of the DSC sample using ITiO was 5.64%, whereas it was 2.73% and 6.47% from DSCs using ITO and FTO, respectively, both at 100 mW/cm2 light intensity [45].

Also the relationship between energy gap & efficiency in dye solar cells was done by Sakina Ibrahim Ali. Four samples of (Ecrchrom Black T, DDTTC, Rohadamin B, Coumarin 500) solar cells were madeby depositing the solution of Day sensitized on ITO Aluminum electrodes by Spin Coatingtechnique and another layer was deposited from dye on a layer of (MEH-PPV).Al was used on the layers to act as anode and ITO as Cathode. A clean glass plate with a thin layer of ITO (Indium Tin Oxide) was needed. The ITO acts as the first part of the solar cell, the first electrode. In this work dye sensitized solar cells made from: Ecrchrom Black T, DDTTC, Rohadamin B, and Coumarin 500, with Al and TTO electrodes were fabricated. The energy gab of these dyes were found using UV Spectrometer. The energy gap for: Ecrchrom Black T, DDTTC, Rohadamin B,

and Coumarin 500 ; were found 2.16 eV ,2.20 eV ,3.27 eV and 3,60 respectively . The V- I characteristics for these cells and their performance were also found. The efficiency: Ecrchrom Black T, DDTTC, Rohadamin B, Coumarin 500 were found 1.66, 1.62, 1.49 and 1.31. It is realized that; the efficiency increased when energy gab decreased .Ecrchrom Black T, DDTTC, Rohadamin B, Coumarin 500 were found 1.66,1.62, 1.49 and 1.31. It is realized that; the efficiency increased when energy gab decreased.

This work shows that the energy gap of the dyes used in dye sensitized solar cell affect the performance and efficiency of the solar cell [46].

Also the relationship between atomic number & efficiency at dye solar cells was done by Sakina Ibrahim Ali. Six samples were prepared by depositing MEH-PPV and using a different electrode Al, Ag and Au to act as an anode were prepared. The V- I curve for all solar cell sample were found by using electric circuit consisting of ammeter, volt meter and power supply. In this work the effect of changing the anode of polymer solar cell on their performance was experimentally investigated .The cells were fabricated from ITO which act as a cathode beside MEH- PPV, Ecrchrom Black T and Rohadamin B dyer. The anodes which care Al, Ag, Au with atomic number 13, 47 and 79 were used. It was found that the efficiency of the solar cell of Al, Ag, Au electrode for Ecrchrom dye are 1.66, 1.59, and 1.58Respectively the efficiency for Rohadamin , Ecrchrom Black T dye are 1.49, 1.48 and 1.46 respectively these results shows clearly that the efficiency increases as the atomic number decreases this conforms with the fact that energy gap increase with the atomic number. This work shows that the electrode type affect polymer solar cell performance. This performance depend on the atomic number of the electrode [47**]**

Also first-principles investigation of the optical properties of crystalline poly (di-n-hexylsilane) was done by W. Y. Ching .He used the orthogonalized linear combination of atomic orbital's (OLCA) method to calculate the electronic

structure of the Pdn6s crystal. This is an all-electron fully self-consistent method based on the LDA of the density functional theory (DFT), and is known for its efficiency and accuracy especially for complex crystals. The optical properties of poly (di-*n*-hexylsilane) are studied by first-principles local-density calculations based on the crystal structure recently determined by x-ray diffraction. The one-dimensional nature of the band, the orbital composition of the states, and the charge distribution of the highest-occupied-molecular-orbitals–lowest unoccupied-molecular-orbitals states on the Si backbone, the effective masses, and the anisotropic optical conductivity are all clearly delineated. (S0163-1829~96-04543-2).In conclusion, the LDA-based first-principles band approach is very effective in elucidating the structure and properties of the polysilane polymers. The present calculation delineates the nature of bonding in one such polymer and unequivocally show that optical properties in the UV region are mainly controlled by the orbital bonding of the Si backbone. It is thus expected that different backbone confirmation can change the HOMO and LUMO state levels and wave functions to give different optical spectra. This is consistent with the notion that thermo chromium in Pdn6s is associated with an order-disorder transition from an all-transto a one at least partly trans-gauche, with the accompanied variations in the structural arrangements of the side chains.

This certainly affects the formation of bond exciton below the CB edge. The present calculation also demonstrates for that the Si 3*d* orbitals are important in the unoccupied states which determine the optical properties in the UV region [48].

Also electrical and optical properties of fluorine doped tin oxide thin films prepared by magnetron sputtering was done by Ziad Y. Banyamin .In this work FTO thin films were deposited onto standard size (5 mm by 25 mm, 1 mm thick) microscope glass slides using a mid-frequency pulsed DC magnetron sputtering technique from loose powder targets. Different fluorine doping levels were

prepared in the tin oxide powder targets in order to study the effect of doping level on the structure and photoelectrical properties of the thin films. Fluorine doped tin oxide (FTO) coatings have been prepared using the mid-frequency pulsed DC closed field unbalanced magnetron sputtering technique in an Ar/O2 atmosphere using blends of tin oxide and tin fluoride powder formed into targets. FTO coatings were deposited with a thickness of 400 nm on glass substrates. No post-deposition annealing treatments were carried out. The effects of the chemical composition on the structural (phase, grain size), optical (transmission, optical band-gap) and electrical (resistivity, charge carrier, mobility) properties of the thin films were investigated. Depositing FTO by magnetron sputtering is an environmentally friendly technique and the use of loosely packed blended powder targets gives an efficient means of screening candidate compositions, which also provides a low cost operation. The best film characteristics were achieved using a mass ratio of 12% SnF2 to 88% SnO2 in the target. The thin film produced was polycrystalline with a tetragonal crystal structure. The optimized conditions resulted in a thin film with average visible transmittance of 83% and optical band-gap of 3.80 eV, resistivity of 6.71 × 10−3Ω·cm, a carrier concentration (Nd) of 1.46 × 1020 cm−3 and a mobility of 15 cm2/Vs.

Transparent conductive oxide SnO2:F thin films have been deposited on glass substrates by the pulsed DC magnetron sputtering technique in an Ar/O2 atmosphere using loosely packed blended powder targets. The thin films were grown at a deposition rate of 27 nm·min−1 and a deposition temperature below170 °C. It was determined that 5.3 at.% fluorine incorporated into the film gave the best electrical behavior. In addition, the XRD structural analysis showed that the crystallinity of the SnO2 samples were improved with the fluorine incorporation and the intensity of the (200) plane ameliorated with the increase in the fluorine concentration up to 5.3 at.% found in the thin film. The average optical transmittance achieved for this coating was 83% across a range of 300

≤λ≤ 900 nm. The detailed analysis of the electrical properties of the thin film as a function of the fluorine doping level revealed that a resistivity as low as6.71 × 10−3Ω·cm was obtained with a fluorine content of 5.3 at.%.This work has shown the ability to grow transparent conductive oxide SnO2: F thin films using a cost effective (no post annealing of samples, and high deposition rate) and environmentally friendly method(no fluorine gas is used and no toxic affluent is produced). This technique is of great advantage for studying the properties of multi component materials and identifying optimum compositions [49].

Also the effect of different dyes on the efficiency of polymer solar cell was done by Omer Abdalla Omer Gassim. In this work polymer cells with different thicknesses and three different type of organic dyes (Rhodamine 6G, Coumarin 500 and Dibenzocyanin 45) are used in fabrication. The effect of the concentration of different organic dye on various electrical and optical properties of the samples produced has been studied. It was found that when the conjugate polymer layer deposition on the slides at low speeds by spin coating technique (increasing the thickness of the conjugate polymer layer), results gave a recognized higher efficiency in the tested cell. The use of the organic dye (DDTTCI) led to improve in efficiency and absorption coefficient of light in the samples used. In addition, the optical absorption spectra were recorded for those samples with a UV -VIS spectrophotometer (model: UV mini-1240) within the wavelength range of 200–800 nm, at room temperature.

The samples show variations in absorption coefficient directly depending on the type of organic dye used as well as the concentration of conjugate polymer. Short-circuit current, open circuit voltage and the fill factor of each sample have been calculated. The efficiency was found in the range of 10.28-1.744% for designed samples.

In this work calculations of IV Characterization and absorbance spectra of conjugated polymers have been made and different types of polymer solar cells have been produced. Five samples of solar cells have been fabricated.

The optical absorbance of these films was measured by UV-VIS spectrophotometer. The samples show a wide range of absorption of the solar spectrum. Sample A5 and sample A2 was recorded the highest absorbance and the lowest absorbance, respectively. For the IV -curve obtained for the conjugate polymer solar cells a curve similar to the curve from the optimal model as described in (I. Montanari, 2002). All samples showed a variation in terms of obtained efficiency ranged between 10.28 % - 3.117 % [50].

Also the effect of exchanging the ZnO and CnO layers on their performance was done by Thowra Abd Elradi Daldowm. In this work two solar cell types were fabricated. The first type is FTO/ CuO/ ZnO/ Al and the second type is FTO/ ZnO/ CuO/ Al. Six samples were prepared from each type. The efficiency for each type was obtained. It was found that the efficiency of FTO/ ZnO/ CuO/ Al is in the range ~0.6×10^{-3}, while the efficiency of FTO/ CuO/ ZnO/ Al is in the range ~2×10^{-3}. The difference may be attributed to the fact that FTO and CnO acts as p-type semiconductor, while ZnO act an n- type semiconductor. Thus the first type acts as pnp component thus have low efficiency, while the second type acts ppn component and have relatively high efficiency.

The results show that the solar cell which is formed from FTO/ CuO/ ZnO/ Al respectively is more efficient and has good performance compared to FTO/ ZnO/ CuO/ Al solar cell. The efficiency can be increased considerably by adding donors to ZnO and acceptors to CuO [51].

Also optical properties of glass and plastic doped by CU was done by Elharam Ali Eltahir Mohammed, Glass and plastic samples are doped with Cu at different concentrations. The results obtained show that increasing Cu concentration

decreases absorption coefficient, refractive index, real and imaginary electric permittivity, whereas energy gap increases. These results surprisingly agree with the theoretical model that treats Cu as an electric dipole.

The results show that the absorption of light by glass can be changed by changing the concentration of Cu. The increase of Cu concentration decrease absorption coefficient. This means that in the design of windows in homes one can enable more light to pass into the room, by decreasing concentration of Cu. It can be also be used in designing sensor and solar cells to improve their performance [52].

Also optical and electrical characteristics of TIO2 – MEH multilayers thin film was done by Tayiser MohiEldin Elmahdi. The optical and electrical properties of TiO2-MEH-PPV double layer was studied when their number is increased. It was found that increasing the number of double layers decreases the energy gap which may result from the effect of the internal MEH electric field that allows some energy levels to enter the energy gap. The absorption also increases when layers were increased which may result from the narrowing of the energy gap. The current however decreases up on increasing the layers which may be related to the increase of electric resistance.

The results show that the energy gap of TiO2 - MEH double layer can be decreased and the absorption can be increased by increasing the number of them. Thus increase of TiO2 - MEH layers decreases current [53].

3.4 Using Gum Arabic in Making Solar Cells by Thin Films Instead Of Polymers

This work was done by Abdelsakhi, three samples of Gum solar cells were made by depositing the Gum Arabic solution on ITO glass by Spin Coating technical, and another layer was deposited from dye on a layer of Gum Arabic .Gold was fabricated on the layers to represent the anode and ITO Cathode. Gum Arabic

based solar cells with Rhodamine 6G were fabricated on indium tin oxide by a spin coater position. Microstructure and cell performance of the solar cells with ITO/ Rhodamine 6G/ Gum Arabic structures were investigated. Photovoltaic devices based on the Rhodamine 6G / Gum Arabic hetrojunction structures provided photovoltaic properties under illumination. Absorption and energy gap measurement of the Rhodamine 6G / Gum Arabic hetrojunction were studied by using UV-VS mini 1240 spectrophotometer and light current-voltage characteristics. The energy levels of the present solar cells were also discussed. The three ITO/Gum/Rhodamine/Au solar cells were produced and characterized, which provided efficiency (η) is (3.8 - 5.1 and 5.2) %. Fill factor (FF) is (0.964 - 0.9462 and 0.973), current density (Jsc) is (2.22 - 4.31 and 4.4) mAcm-2 and Open – circuit voltage (Voc) is (1.22 -1.25 and 1.209) V. This could be used at larger scale in promoting efficiency of solar cells. The application of conducting Arabic Gum to optoelectronic devices such as solar cell, light emitting diodes, and electrochemical sensors are of practical significance, because the Arabic Gum mixture can be easily prepared and modified by rich chemical procedures to meet optical and electronic requirements .This solar cell is cheap can be easily fabricated. It efficiency is relatively large [54].

3.5 Solar Storm Threat Analysis

This work was done by James A. Marusek. Most solar storms produce only minor disquieting effects on Earth. Typically one might expect short-term electrical power blackouts, short lived communication outages, rerouting of aircraft, loss of a few satellites and a beautiful “aurora borealis” in the nights sky from a large solar storm .But as the intensity of a solar storm increases like a wild beast, the storm can begin to develop the capacity to create a major disaster on Earth. The difference in solar storm intensity is like the difference between being hit with a tropical rainstorm and being devastated by a Category 5 hurricane. The solar storm of 1-2 September 1859, which began with a solar flare so strong that it was

subsequently named the Carrington Flare, was such a beast. Oak Ridge National Laboratories estimated that only a solar storm just slightly stronger than the 13 March 1989 storm (Dst = 589 nT) would have the capacity to produce a cascading blackout involving the entire Northeastern sector of the United States. So the question is "What damage would a spawned geomagnetic storm like the one of 2 September 1859 (Dst = 1,760 nT) bring?" Would it simultaneously degrade and damage several unique large electrical transformers at key electrical generating stations taking down the massive power grid? Would the long lead-time required to manufacture and install replacement equipment result in major yearlong electrical blackouts, rolling blackouts and brownouts? How would a long-term lack of stable electricity affect advanced civilization? This work dissects and analyzes the various threats created by Great solar storms.

Most solar storms produce only minor disquieting effects on Earth. Typically one might expect short-term electrical power blackouts, short-lived communication outages, rerouting of aircraft, loss of a few satellites and a beautiful "aurora borealis" in the nights sky from a large solar storm. But as the intensity of a solar storm increases it develops the capacity to create a major disaster on Earth. A Great solar storm has the potential of seriously damaging the North American electrical power grid. The resulting blackout will be focused on the northern tier of states and the East and West coast of the U.S. and throughout Canada. The damaged equipment in the power infrastructure would generally have a replacement lead time of over a year due to its uniqueness. But the scope of the outage will be so great that governments will quickly elevate its repair to the level of a national imperative. As a result, restoration that might normally take over a year will occur in a matter of weeks. Critical elements affected by the blackout will include water, sewage, commerce, industry, banking, transportation, communications, and in the winter, heating. Because modern society relies so heavily on sophisticated technology, a long-term blackout will have a very

profound effect on the fabric of society. Many satellites will be destroyed or severely degraded. The loss will primarily target communications. The lead time to construct and replace these assets will be measured in terms of years [55**].**

3.6 Applications of Oxide Coatings in Photovoltaic Devices

This work was done by Sonya Calnan. Metalloid and metal based oxides are an almost unavoidable component in the majority of solar cell technologies used at the time of writing this review. Numerous studies have shown increases of ≥1% absolute in solar cell efficiency by simply substituting a given layer in the material stack with an oxide. Depending on the stoichiometry and whether other elements are present, oxides can be used for the purpose of light management, passivation of electrical defects, photo-carrier generation, charge separation, and charge transport in a solar cell. In this review, the most commonly used oxides whose benefits for solar cells have been proven both in a laboratory and industrial environment are discussed. Additionally, developing trends in the use of oxides, as well as newer oxide materials, and deposition technologies for solar cells are reported.

Oxides are an important component of PV cells and shall continue to be so in the future. Due to the diverse applications of oxides in PV cells, only a snap shot can be made of the range of devices that have been explored. On the one hand, we have the traditional oxides for various functionalities and on the other, new oxide materials are being introduced for use in PV. While the transparent conducting oxides of indium, zinc and tin are important as electrodes in most PV cell technologies, TiO_2 has become the model material for PV cells based on charge transfer to a sensitized semiconductor. The oxides of silicon and aluminum, both members of the semi-metal group, when highly insulating can be used for passivation due to their high dielectric constant. The transition metal oxides with high work functions are now routinely used for organic PV cells as electrode buffer materials to maximize the cell voltage and to prevent leakage currents.

Other oxides, such as those of copper and lead have been used as absorber materials. More exotic multiparty oxides such as the ferroelectric Perovskite $BiFeO_3$ and $KNbO_3$ are used as absorbers with the promise of high cell voltage. Lanthanide host oxides and lanthanide doped oxides have been introduced as wide band spectral converters to enhance the spectral response of PV cells beyond the normal absorption band of the absorber material. Much as this review has focused on examples of applications of oxide materials where PV cell performance has been experimentally demonstrated, the contribution and importance of theoretical calculations towards these and future developments cannot be overstated [56].

Chapter Four

Experimental work

4.1 Introduction

This chapter is concerned with the experimental work. This includes sample preparation, apparatus, theory and the experimental work set up. In this work solar cell types with different dyes were fabricated.

4.2 The Materials of an Organic Solar Cell

4.2.1 Polymer

Polymer is a Greek phrase which means many parts. Large molecules made of repeating units of smaller molecules. Small molecules are called “monomers" monomers link together like a chain resulting in new and exciting properties [57].

Conjugated polymers are organic macromolecules with alternating single and double bonds. Conjugated polymers are organic semiconductors, the semiconducting behavior being associated with the pi-molecular orbitals delocalized along the polymer chain. Due to the 2sp hybridization of the electron system, conjugated polymers are mostly planar, extended macromolecules. They combine the optical and electrical properties with the mechanical advantages for preparation of optoelectronic devices .There is one unpaired pz-electron per C-atom, which forms pi-pi* conduction and valence bands in the macromolecule due to the fact, that they describe a one-dimensional crystal[58].The Noble Prize in Chemistry 2000 was awarded jointly to Alan J. Heeger , Alan G. MacDiarmid and Hideki Shirakawa "for the discovery and development of conductive polymers", This discovery led, subsequently, to the discovery of electroluminescence in a poly(p-phenylenevinylene) (PPV) [59]. In 1990 the first light-emitting products based on electroluminescence in conjugated polymers

have already been launched at the consumer market by Philips (The Netherlands) in 2002, whereas light-emitting products based on conjugated molecules have been introduced by the joint venture of Kodak and Sanyo (Japan). Going from discovery to product within a little bit more than one decade truly holds a huge promise for the future of plastic electronics. Other emerging applications are coatings for electrostatic dissipation and electromagnetic-interference shielding [60]. Conjugated polymers and molecules have the immense advantage of facile, chemical tailoring to alter their properties, such as the band gap. Conjugated polymers combine the electronic properties known from the traditional semiconductors and conductors with the ease of processing and mechanical flexibility of plastics. In this research was used poly (2-methoxy-5-(2'-ethyl-hexyloxy)-1.4 phenylene) (MEH-PPV) shown in fig (4.1) due to the corresponding internal quantum efficiency .The absorbed photons to electrons, is estimated to be nearly 100% in the short circuit case. The main limiting factor towards higher efficiencies is the spectral mismatch of the active layer absorption, with a maximum around 500 nm, to the terrestrial solar spectrum with a maximal photon flux between 600 and 800 nm [61]. Therefore, the use of low band gap {Eg~ 2.0 eV}. Polymers is a viable route to increase the amount of absorbed photons and consequently the power efficiency of solar cells [62]. Characterized polymers that can be turned into solids or semi-conductive for electricity as we mentioned earlier, and to make solar cells must first add a certain percentage of oxidizing substances or shorthand to become Article polymeric. Similar properties semiconductors inorganic and lead impurities to situations within the scope of the gap between the bands valance band conduction has found that the energy gap of the semiconductor in some polymers ranging from (1.5-3 eV) and thus wider than the gap in the energy inorganic materials that range where the energy gap between 0.1-2.2 eV in and fit so with photon energy in the visible range of the solar radiation [63].

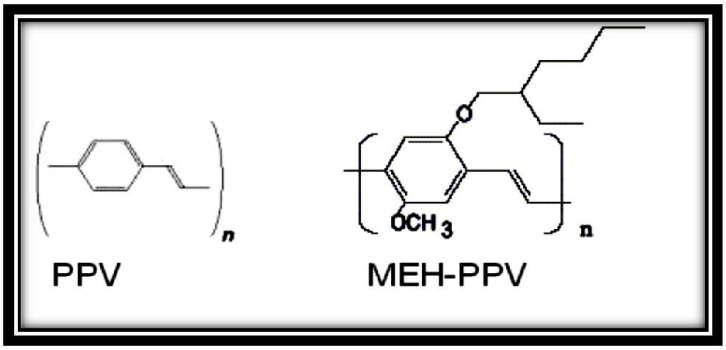

Figure (4.1) the two figures is the monomer of MEH-PPV (right) and the monomer of PPV (left).

4.2.2 Indium Tin Oxide (ITO)

Indium Tin Oxide (ITO) is a transparent conductive material. It is a mixture of indium oxide (In_2O_3) and tin oxide(SnO_2). ITO was used as one of the electrodes in the solar cell .ITO can absorb light at the same wavelength as MEH-PPV. This is important because only the light absorbed by MEHPPV may result excitations [64].

4.2.3. (DDTTCI) Dye

The dye(DDTTCI)Constitution[3,3'-Diethyl4,4',5,5'dibenzothiatricarbocyanine Iodide Hexadibenzocyaini 45C33H29N2S2I· MW: 644.43] Characteristics Lamb dachrome® number: 9280CAS registry number: Appearance: bronze colored, crystalline solid Absorption maximum (in ethanol): 798 nm Molar absorptivity: $19.6 \times 10^4 \text{L mol}^{-1}\text{cm}^{-1}$ Fluorescence maximum, this dye is shown in fig (4.2).

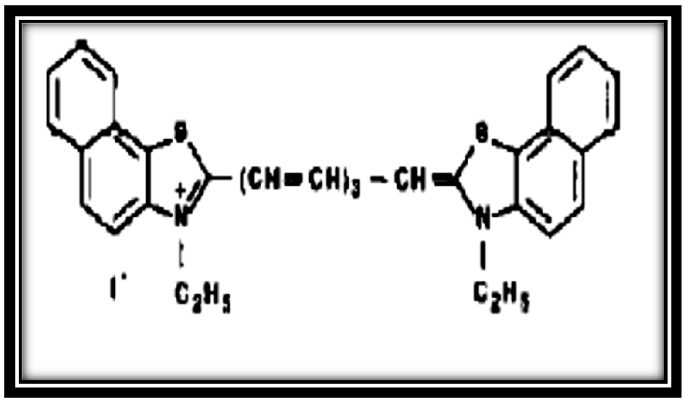

Figure (4.2) the structure of (DDTTCI) dye.

4.2.4 (Ecr - chrome Black T) Dye

This dye is Preferred IUPAC name: sodium 1-[1-hydroxynaphthylazo]-6-nitro-2-naphthol-4-sulfonateSystematicname:sodium4-[2-(1-hydroxynaphthalen-2yl)hydrazin-1-ylidene]-7-nitro-3-oxo-3,4-hydronaphthalene-1-sulfonate Other Names:Sodium4-[2-(1-hydroxynaphthalen-2-yl)hydrazin-1-ylidene]-7-noxonaphthalene-1-ulfonate; Ecr-chrome Black T; ET-Eriochrome Black T is a complex metric indicator that is part of the complex metric titrations see fig(4.3), e.g. in the water hardness determination process. It is an azo dye. Eriochromeis a trademark of Ciba-Geigy. In its protonated form, Eriochrome Black T is blue. It turns red when it forms a complex with calcium, magnesium, or other metal ions [65].

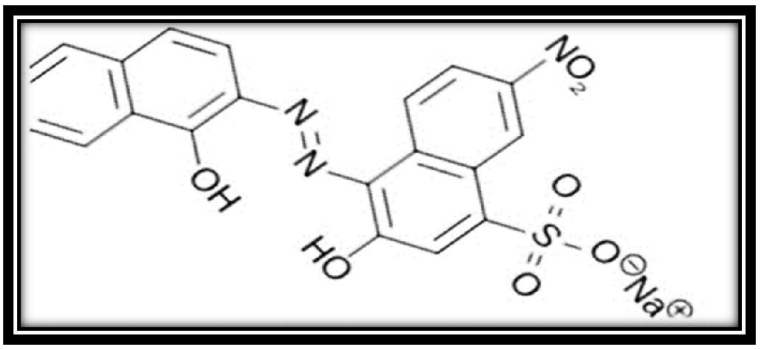

Fig (4.3) Ecr - chrome Black T structure

4.2.5 Zinc oxide (ZnO)

The emphasize here will be on the fundamental properties of ZnO as shown in fig(4.4), like growth, electrical and optical properties, since the potential for optoelectronic devices based on ZnO is also one of the main motivations for the present work. ZnO is a direct wide band-gap (3.37eV at room temperature) II-VI binary compound semiconductor and crystallizes in three forms: hexagonal quartzite, cubic zinc blend, and the rarely observed cubic rock salt [66]. The hexagonal quartzite structure of ZnO is the most common phase having a crystal structure C6v or P63mc, which occurs almost exclusively at ambient conditions

[67, 68]. The quartzite ZnO structure consists of alternating zinc (Zn) and oxygen (O) atoms is shown in Figure (4.3). The ZnO structure has polar surface (0001) which is either Zn or O terminated and non-polar surfaces (1120) and (1010) possessing an equal number of both atoms. The polar surface of ZnO is highly metastable in nature and is responsible for several unique and astonishing properties including piezoelectric properties, it also play a key role in column growth, favorable for etching due to higher energy. The polar surface is also known to possess different physical and chemical properties [69].

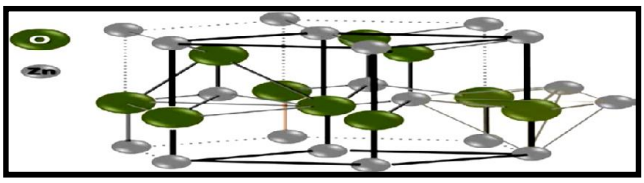

Figure (4.4) Crystal structure of hexagonal quartzite ZnO

4.2.6 Copper (II) Oxide

Among other compound semiconductors, copper oxide is of great interest in semiconductor physics. Copper forms two well-known stable oxides, cupric oxide (CuO) and cuprous oxide (Cu_2O). These two oxides have different physical properties, different colors, crystal structures and electrical properties. There are many reasons why CuO is chosen for sensing applications. CuO has monoclinic structure belong to space group 2/m, it displays a wealth of interesting properties, it is abundant, nonhazardous source materials, and it can be prepared by low cost solution methods which are the key issues for sensing applications. Figure (4.4) shows the monoclinic structure of the CuO.

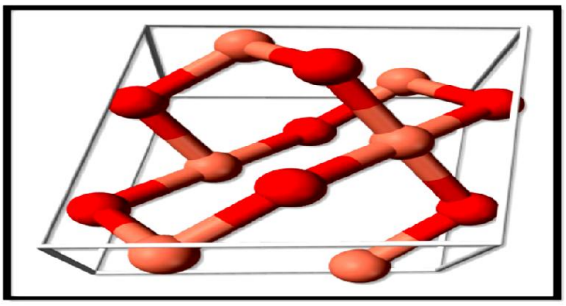

Figure (4.5) Copper (II) oxide (CuO) crystal structure

4.3 Methods

Four samples of solar cells were made by depositing the solution of dye (Ecrchrom Black T, DDTTC) and tow samples mead by (ZnO and CuO) on ITO by Spin Coating technic, and another layer was deposited from dye on a layer of (MEH-PPV). Aluminum (Al) is electrode was fabricated on the layers to acts anode and ITO Cathode. The fabrication process started by preparing the MEH-PPV and the dye of interest then spin coated it indium tin oxide glass. Aluminum (Al) electrode was used to complete the formation of solar cell. The formed cells were characterized by Ultra violet-visible spectroscopy. Electrical circuit containing the (voltmeter and Ammeter and a light source Lamp). Was need to study performance .The solar cell was exposed to light and the current and voltages of the cell recorded there UV spectrometer was need to display absorption spectrum.

For the purpose of the present study Electronic transport in the (Four samples of solar cells were made by depositing the solution of dye (Ecrchrom Black T, DDTTC) and tow samples mead by (ZnO and CuO_2) on ITO and aluminum (Al) is electrodes) , and another layer was deposited from dye on a layer of (MEH-PPV)) devices is studied via current density voltage (*J-V*) curves, taken using a 2400 Keithley source meter by sourcing voltage across the ITO (positive) and aluminum (negative) Electrodes and measuring the resulting current density. Due

to the reversed internal field, measurements on the ITO/PEDT/MEHPPV/ Al devices are taken by sourcing ITO positive and Al negative.

4.4 Apparatus:

Sex samples of solar cell (2×1) cm with different types,2 natural dyes,2 chemical dyes , 1 plug-in board A4 576 764,1 set of ten bridging plugs 501 48,1 pair of board holders 576 771 , 1 microvolt-DMM- voltmeter, KETHLEY-USA- 177 DC,1electrometer- ammeter, KETHLEY-USA- 642 DC, 1 halogen lamp housing, 12 V, 50/100 W 450 64 , rheostat -Albert van der perk nV Rollerdom-No-464151-27Ω-5.2A, light OF intensity (scouts light, power of 1000 w),Connecting wires .The purpose of this experiment is to find out the fill factor and efficiency of polymer solar cell by using Four samples with different types of dyes and tow samples mead by (ZnO and CuO) on ITO by Spin Coating technic. The spin coating see Fig (4.5) technique device was remove and surface was washed by distilled water and methanol, then rinsed with Acetone and dried, the ITO Glass was put in spin coating. The prepared of polymer (MEH–PPV) solution was spin coated on the ITO glass substrate for 60 sec, and prepared of dye solution was spin coated on the polymer at about 600 rpm for 60 sec in order to yield a thin uniform film . Finally Silver strips were evaporated on top of the thin film.

Measures absorbance, emission and permeability. The range from 190-1100nm range for registration -3.99-3.99.Named UV mini 1240 spectrophotometer made in a Japanese company called Shimadzu measures two types of fluids and can measure the solids in the form of slides. The device components are: light source – a cell sample – uniform wavelength – Scout – Screen. The working principle of the device .Each of the articles has a characteristic absorption of a specific wavelength. Any material has a certain extent of absorption to unchangeable but the material properties change works on the principle Ber -lambert based on assumptions:

*Absorbance is directly proportional to the concentration.

*Absorbance is directly proportional to the length of the optical path within the sample.

Figure (4.6) spin coating device.

Figure (4.7) UV spectrometer device.

4.5 Theory:

While in previous organic photocells the polymers conducted holes and the acceptor conducted electrons, the roles are reversed in this photocell. This means the heavier charge is transported along the fastest pathway. For MEH-PPV, the fastest transport path is along the polymer backbone, with cross-chain transport being orders of magnitude slower. Ideally, polymers and nanotubes would be aligned perpendicular to the electrodes to provide the most rapid transport path possible. The key factors for determining how efficient our devices will be are the electron mobility within our polymer and the hole mobility within the CNTs.

The highest recorded electron mobility for MEH-PPV at room temperature is $3.3x10^{-7}$ cm^2/Vs while the average hole mobility for CNT's at room temperature is around 3000 cm^2/Vs. Note the latter value is 10 orders of magnitude above the best polymer mobility indicating it would be unlikely to be a rate limiting (15-19). Numerous papers have shown the electron mobility in MEH-PPV can be equated by:

$$\mu = \mu_o \, e^{0.89\gamma\sqrt{E}} \qquad (4.1)$$

Where μ_o is the zero field mobility (for MEH-PPV this value has been determined to be $(1 \pm 0.5) x10^{-7}$ cm^2/Vs) and γ is the electric field coefficient (for MEH-PPV this value is given by $(4.8 \pm 3) x10^4$(m/V).5). E is the electric field applied to the device by the differing work functions of our electrodes. From this equation we can use that mobility to find the current density within the polymer [68]:

$$J = \frac{9}{8} \, \varepsilon\mu E^2/L \qquad (4.2)$$

Where ε is a constant equal to $3.1 \times 10^{-11} C^2/(Nm^2)$ and L is the thickness of the polymer. From this equation it is simple to predict that reducing the thickness of the device will produce more current.

4.6 Setup:

- The solar cell into the plug-in board was plugged, and the upper negative pole to the lower positive pole were connected using two bridging plugs (series connection of four solar cells).
- The potentiometer as a variable resistor was plugged, and connected it to the solar battery using bridging plugs.
- The ammeter was connected in series with the solar battery and the variable resistor. The measuring range was selected 100×10^{-11}A DC.

- The micro voltmeter was connected in parallel to the solar cell.
- The scouts light lamp was connected to the transformer, and aligned it So that the solar cell is uniformly irradiated.

4.7 Carrying out of the experiment:

- The circuit was closed, first shorting the variable resistor with an additional bridging plug, and choose the distance of the halogen lamp so that the short circuit current was determined.
- The shorting bridging plug was removed, and increases the terminal voltage or decrease the current, respectively, step by step by changing the load resistance. For each step the current and the voltage were read, and take them down.
- Then interrupt the circuit, and measured the open-circuit voltage.
- Repeat the series of measurements by change load resistance.

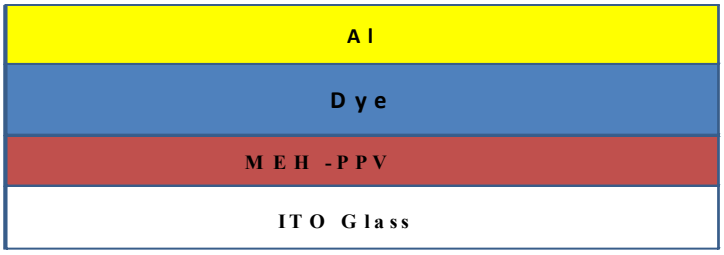

Figure (4.8) samples of solar cells were made by depositing the solution of dye (Ecrchrom Black T, DDTTC) on ITO and Aluminum (Al) is electrodes) , and another layer was deposited from dye on a layer of (MEH-PPV).

Chapter Five

Results, Discussion, conclusion and Recommendations

5.1 Results

Photovoltaic devices of the structure ITO/ MEH-PPV / dyes /Al, as shown in Fig(4.8), are constructed by spin cute first a different dyes and then the photoactive polymer MEH-PPV over indium tin oxide ITO patterned glass. The dyes (DDTTC – Ecrochrom black T- Cu O and ZnO). After spin cute, the dyes under atmospheric pressure to convert the film structure to crystalline. As an alternative to the dyes film, a solution of the dyes deposited via spin casting. The slide is next brought into a dry nitrogen atmosphere glove box and cleaned prior to the deposition of the MEH-PPV polymer in p-xylene solvent via spin coating.

Electronic transport in the ITO/ MEH-PPV / dyes /Al devices is studied via current density voltage (J-V) curves, taken using a 2400 Keithley source meter by sourcing voltage across the ITO positive and aluminum(Ag and gold) negative Electrodes and measuring the resulting current density. These J-V curves are taken both in the dark and under white illumination provided by a halogen source through the ITO electrode. Charge traps, the devices are transferred out of the glove box inside of a sealed test chamber. They therefore remain under the same dry nitrogen atmosphere throughout the photo action current spectra measurements. Reference spectra are taken using a calibrated silicon solar cell.

Absorption spectra are taken with U-V spectrometer and at last atomic magnetic field scanning (AFM) roughness images as shown in fig (5.39), (5.40), (5.41) and fig (5.42).

For solar cell devices of the structure (ITO/ Ecrchrom Black T/ MEH-PPV/ Al), The relation between absorbance and wavelength of MEH-PPV + Ecrchrom Black T shows in Fig (5.1), The rapid increase of the absorption in the low

wavelength and sudden increase in special wavelength, this is refer to electronic transition, and this increase is continuous with the increase of photon energy. The range of absorption beak wavelengths for Ecrchrom Black T was obtained at300 nm and 500 nm respectively and absorption of visible radiation 380 nm (violet)-750 nm (red).

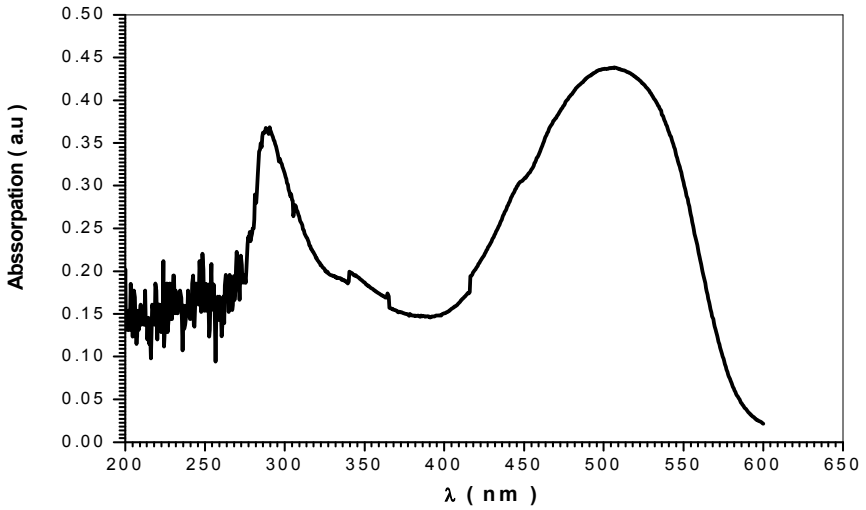

Figure (5.1) shows the relation between absorbance and wavelength of MEH-PPV + Ecrchrom Black T in room temperature.

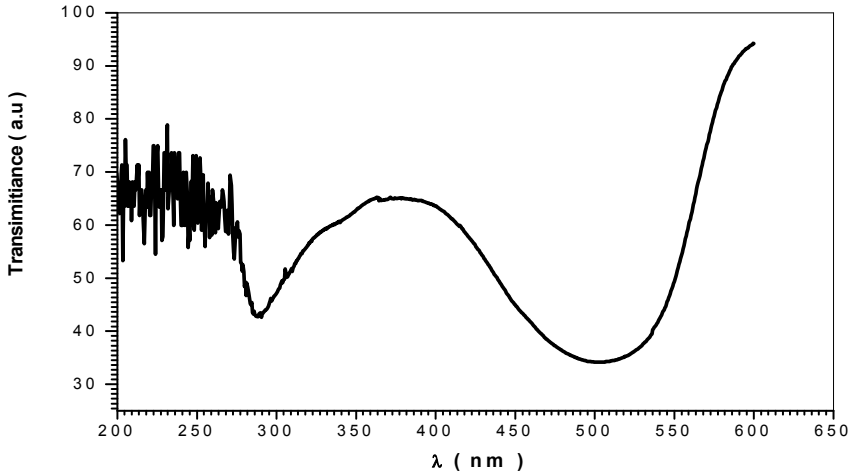

Figure (5.2) shows the relation between transparent and wavelength of MEH-PPV + Ecrchrom Black T.

The optical energy gap (Eg) value of MEH-PPV + Ecrchrom Black T thin films as shown in Fig (5.3). It has been calculated by the relation $(\alpha h\upsilon)^2 = C(h\upsilon - Eg)$ where (C) is constant. By plotting $(\alpha h\upsilon)^2$ vs photon energy ($h\upsilon$). The intersection of the straight line with the $h\upsilon$-axis determines the optical band gap energy Eg, The value of (Eg) obtained was 2.15 eV

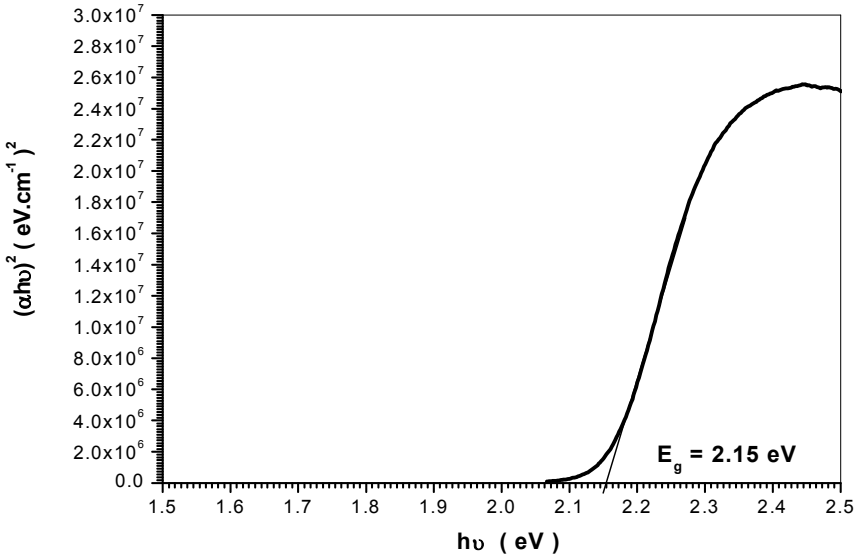

Figure (5.3) the optical energy gap (Eg) value of MEH-PPV + Ecrchrom Black T thin films.

Typical I-V curve of the MEH-PPV + Ecrchrom Black T solar cell for Al electrode as shown in Fig (5.4). It was explain many parameters for cell (Isc), (Voc), (Imax) and (Vmax), short circuit current (Isc) that current passes through the junction under elimination when the voltage is equal to zero. It is directly related to the number of photons of light being absorbed by the cell. open circuit voltage Voc is the applied voltage at which the current density is zero under illumination is determined by the difference between the quasi-Fermi energy level of the (Eriochrome black T = 2.16 eV 'DDTTC = 2.2 eV ' Cu O = 2.9 eV and ZnO = 3.6 eV)and the work function of the Al electrode or the HOMO level of the MEH-PPV In our system, the Al electrode work function 4.08 eV(for silver

Ag electrode work function =4.26 eV and gold Au electrode work function= 5.1 eV) forms an early Ohmic contact with the HOMO of MEH-PPV 5.3eV.other parameters for Ag and Au electrodes is shows in fig(5.5)and fig(5.6) respectively

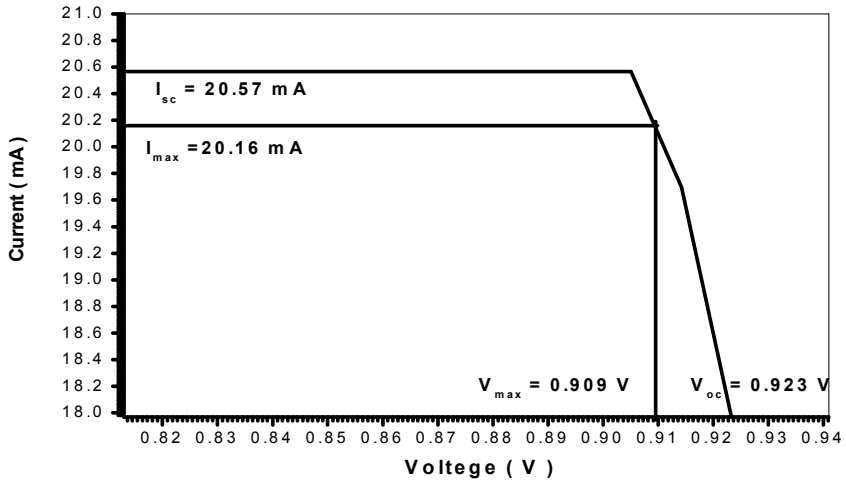

Figure (5.4) Typical I-V curve of the cell of MEH-PPV + Ecrchrom Black T thin films for Al electrode.

Table (5.1) Typical I-V riding of the cell of MEH-PPV + Ecrchrom Black T thin films for Al electrode.

Voltage (V)	Current (mA)
0.99726	**22.17391**
1.01555	**22.17391**
1.03385	**22.17391**
1.043	**22.17391**
1.05215	**22.17391**
1.0613	**22.17391**
1.08875	**22.17391**
1.0979	**21.30435**
1.10704	**19.56522**

From fig (5.5) it clear show that when was changed the electrode from Al to Ag electrode the parameters value increase.

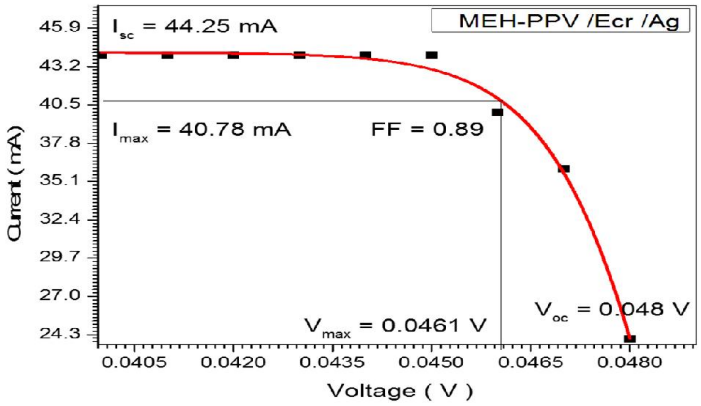

Fig (5.5) Typical I-V curve of the cell of MEH-PPV + Ecrchrom Black T thin films for Ag electrode.

Table (5.2) Typical I-V riding of the cell of MEH-PPV + Ecrchrom Black T thin films for Ag electrode.

Voltage (V)	**Current (mA)**
0.04	**44**
0.041	**44**
0.042	**44**
0.043	**44**
0.044	**44**
0.045	**44**
0.046	**40**
0.047	**36**
0.048	**24**

From fig (5.6) it clear show that when was changed the electrode from Al to Au electrode the parameters value increase.

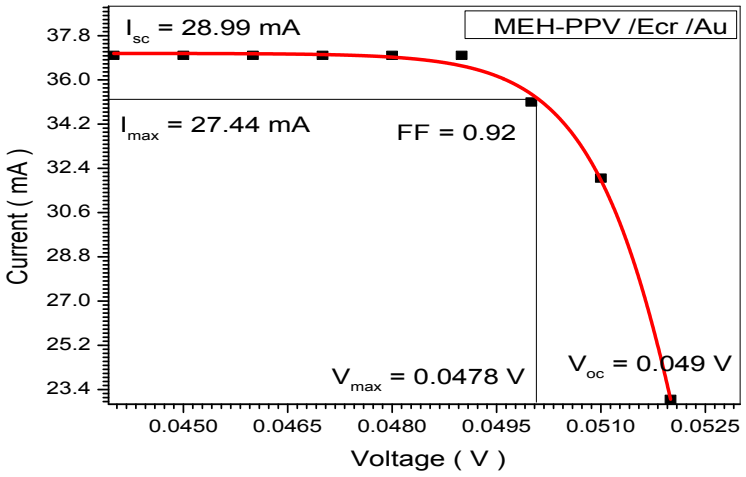

Figure (5.6) Typical I-V curve of the cell of MEH-PPV + Ecrchrom Black T thin films for Au electrode.

Table (5.3) Typical I-V riding of the cell of MEH-PPV + Ecrchrom Black T thin films for Au electrode.

Voltage (V)	**Current (mA)**
0.044	**37**
0.045	**37**
0.046	**37**
0.047	**37**
0.048	**37**
0.049	**37**
0.05	**35.1**
0.051	**32**
0.052	**23**

The relation between absorbance and wavelength for Ecrchrom Black T + MEH-PPV shows in Fig (5.7), The rapid increase of the absorption in the low wavelength and sudden increase in special wavelength, this is refer to electronic transition, and this increase is continuous with the increase of photon energy. The range of absorption beak wavelengths for Ecrchrom Black T was obtained at300 nm and 500 nm respectively.

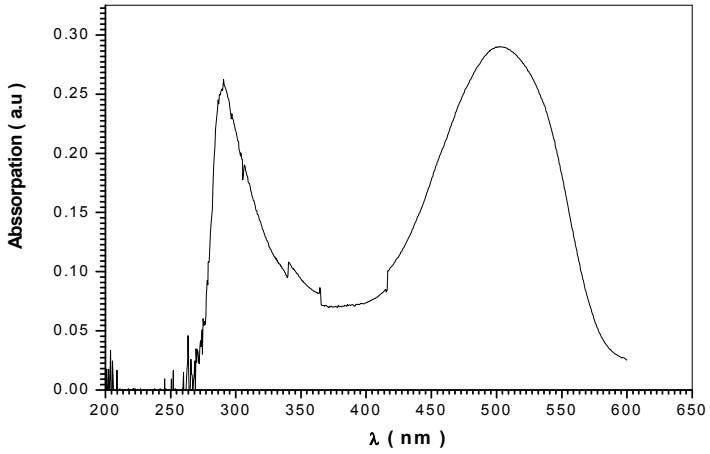

Figure (5.7) shows the relation between absorbance and wavelength of Ecrchrom Black T + MEH-PPV.

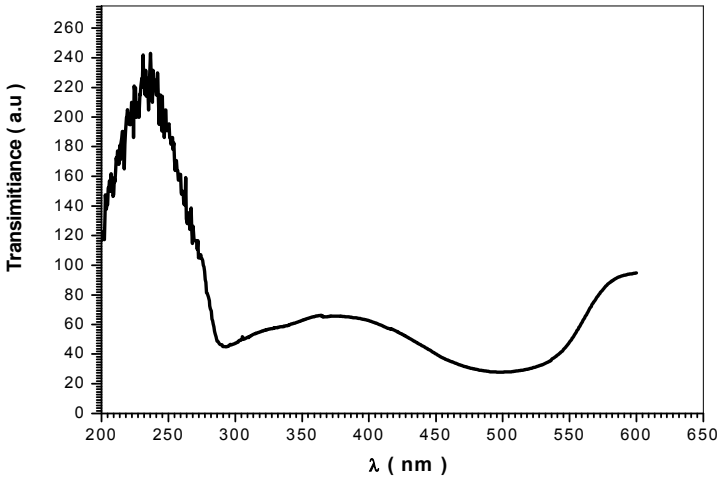

Figure (5.8) shows the relation between transparent and wavelength of Ecrchrom Black T + MEH-PPV.

Fig (5.9) shows the optical energy gap (Eg) value of Ecrchrom Black T + MEH-PPV thin films. The value of (Eg) obtained was 2.16 eV.

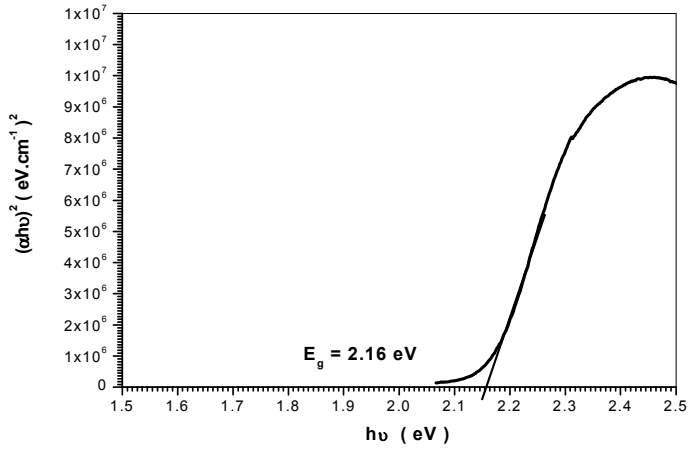

Figure (5.9) the optical energy gap (Eg) value of Ecrchrom Black T + MEH-PPV thin films.

Typical I-V curve of the Ecrchrom Black T + MEH-PPV solar cell for Al electrode as shown in Fig (5.10). It was explain many parameters for cell (Isc), (Voc), (Imax) and (Vmax).

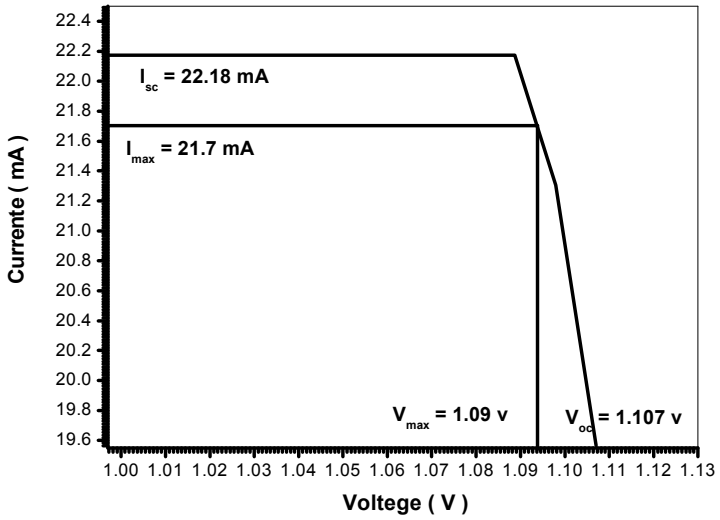

Figure (5.10) Typical I-V curve of the cell of Ecrchrom Black T + MEH-PPV thin films for Al electrode.

Table (5.4) Typical I-V riding of the cell of Ecrchrom Black T + MEH-PPV thin films for Al electrode.

Voltage (V)	Current (mA)
0.96461	**20.79891**
0.9829	**20.79891**
1.0012	**20.79891**
1.01035	**20.79891**
1.0195	**20.79891**
1.02865	**20.79891**
1.0561	**20.79891**
1.06525	**19.92935**
1.07439	**18.19022**

From fig (5.11) it clear show that when was changed the electrode from Al to Ag electrode the parameters value increase.

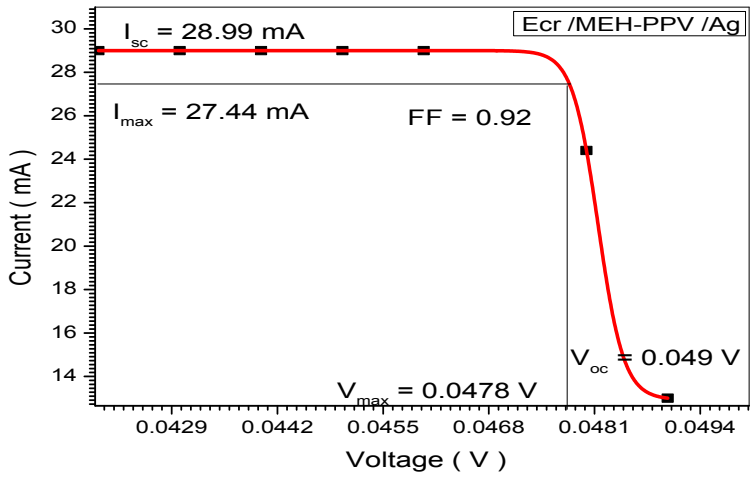

Figure (5.11) Typical I-V curve of the cell of Ecrchrom Black T +MEH-PPV thin films for Ag electrode.

Table (5.5) Typical I-V riding of the cell of Ecrchrom Black T + MEH-PPV thin films for Ag electrode.

Voltage (V)	Current (mA)
0.042	**29**
0.043	**29**
0.044	**29**
0.045	**29**
0.046	**29**
0.048	**24.4**
0.049	**13**

From fig (5.12) it clear show that when was changed the electrode from Al to Au electrode the parameters value increase.

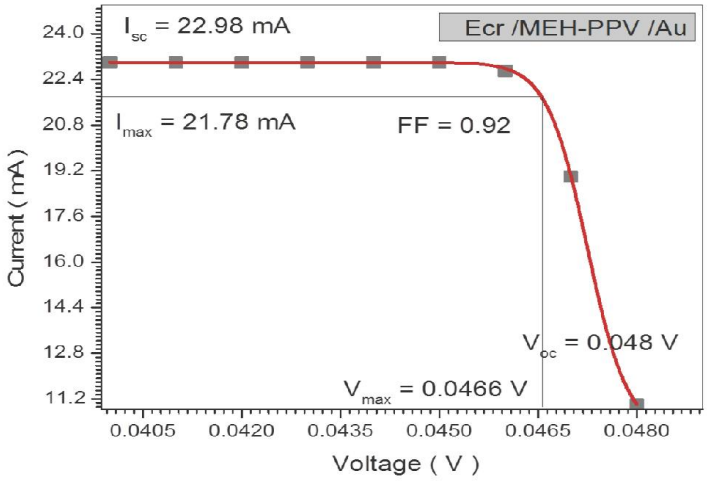

Figure (5.12) Typical I-V curve of the cell of Ecrchrom Black T +MEH-PPV thin films for Au electrode.

Table (5.6) Typical I-V riding of the cell of Ecrchrom Black T + MEH-PPV thin films for Au electrode.

Voltage (V)	Current (mA)
0.04	**23**
0.041	**23**
0.042	**23**
0.043	**23**
0.044	**23**
0.045	**23**
0.046	**22.7**
0.047	**19**
0.048	**11**

Fig (5.13) shows the relation between absorbance and wavelength of CuO +ZnO. The rapid increase of the absorption in the low wavelength and decrease in special wavelength, this is refer to electronic transition, and this decrease is continuous with the decrease of photon energy. The range of absorption beak wavelengths for CuO +ZnO was obtained at330 nm.

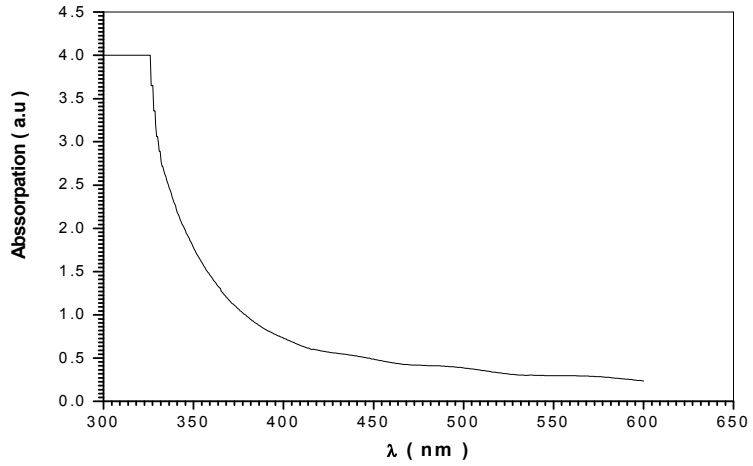

Figure (5.13) the relation between absorbance and wavelength of CuO +ZnO.

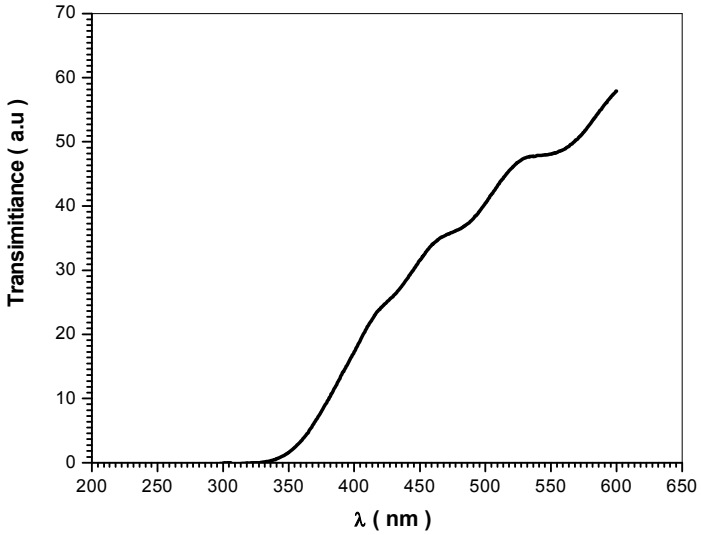

Figure (5.14) shows the relation between transparent and wavelength of CuO +ZnO.

Fig (5.15) shows the optical energy gap (Eg) value of CuO +ZnO thin films. The value of (Eg) obtained was 3. 6 eV.

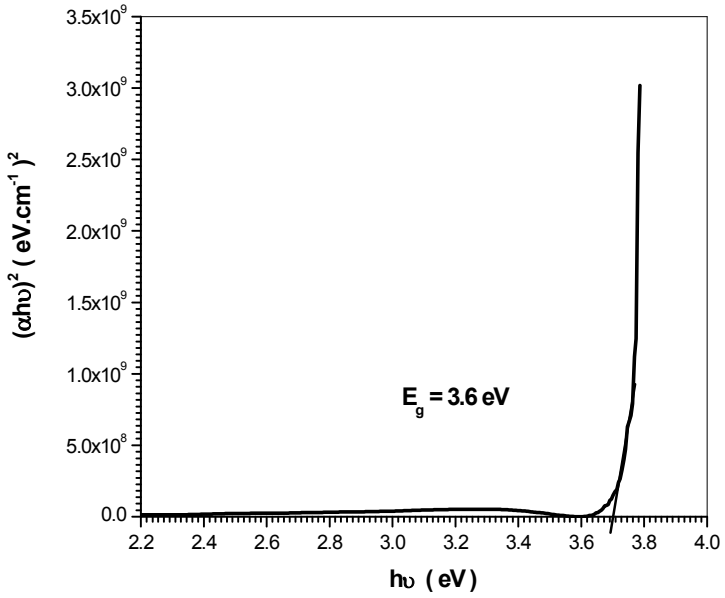

Figure (5.15) the optical energy gap (Eg) value of CuO +ZnO thin films.

Typical I-V curve of CuO +ZnO solar cell for Al electrode as shown in Fig (5.16). It was explain many parameters for cell (Isc), (Voc), (Imax) and (Vmax).

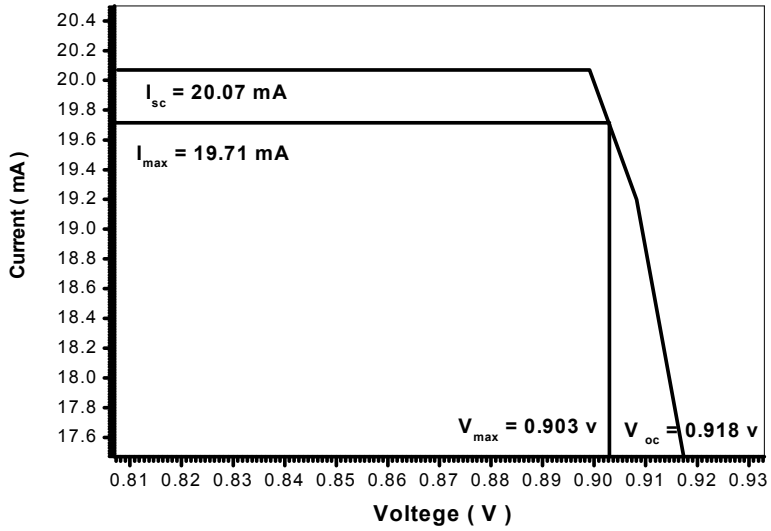

Figure (5.16) Typical I-V curve of the cell of CuO +ZnO thin films for Al electrode.

Table (5.7) Typical I-V riding of the cell of CuO +ZnO thin films for Al electrode.

Voltage (V)	Current (mA)
0.81361	**20.56491**
0.8319	**20.56491**
0.8502	**20.56491**
0.85935	**20.56491**
0.8685	**20.56491**
0.87765	**20.56491**
0.9051	**20.56491**
0.91425	**19.69535**
0.92339	**17.95622**

From fig (5.17) it clear show that when was changed the electrode from Al to Ag electrode the parameters value increase.

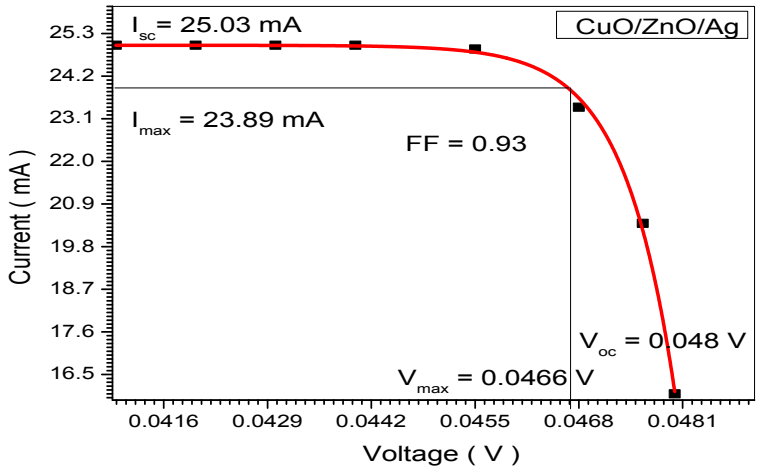

Figure (5.17) Typical I-V curve of the cell of CuO +ZnO thin films for Ag electrode.

Table (5.8) Typical I-V riding of the cell of CuO +ZnO thin films for Ag electrode.

Voltage (V)	Current (mA)
0.041	**25**
0.042	**25**
0.043	**25**
0.044	**25**
0.0455	**24.9**
0.0468	**23.4**
0.0476	**20.4**
0.048	**16**
0.041	**25**

From fig (5.18) it clear show that when was changed the electrode from Al to Au electrode the parameters value increase.

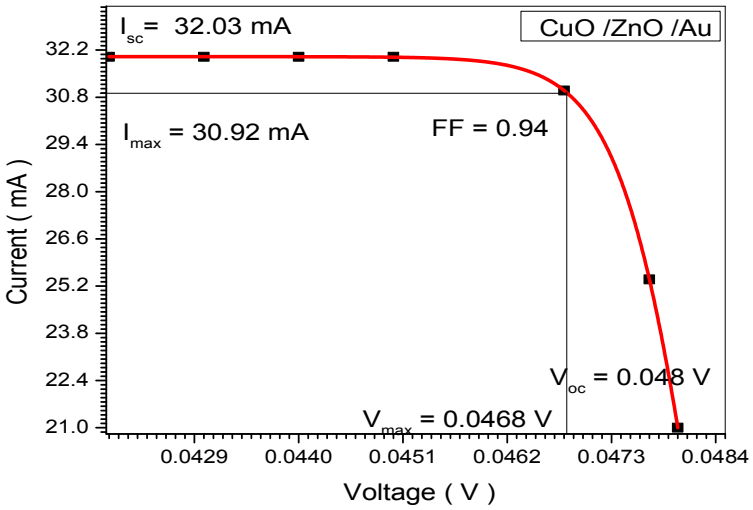

Figure (5.18) Typical I-V curve of the cell of CuO +ZnO thin films for Au electrode.

Table (5.9) Typical I-V riding of the cell of CuO +ZnO thin films for Au electrode.

Voltage (V)	**Current (mA)**
0.042	**32**
0.043	**32**
0.044	**32**
0.045	**32**
0.0468	**31**
0.0477	**25.4**
0.048	**21**
0.042	**32**

Fig (5.13) shows the relation between absorbance and wavelength of ZnO + CuO. The rapid increase of the absorption in the low wavelength and decrease in special

wavelength, this is refer to electronic transition, and this decrease is continuous with the decrease of photon energy. The range of absorption beak wavelengths for ZnO + CuO was obtained at290 nm.

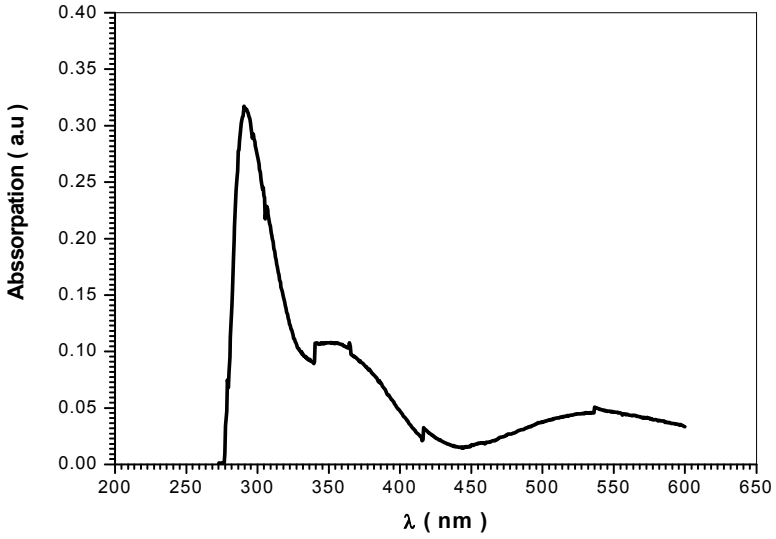

Figure (5.19) shows the relation between absorbance and wavelength of ZnO + CuO.

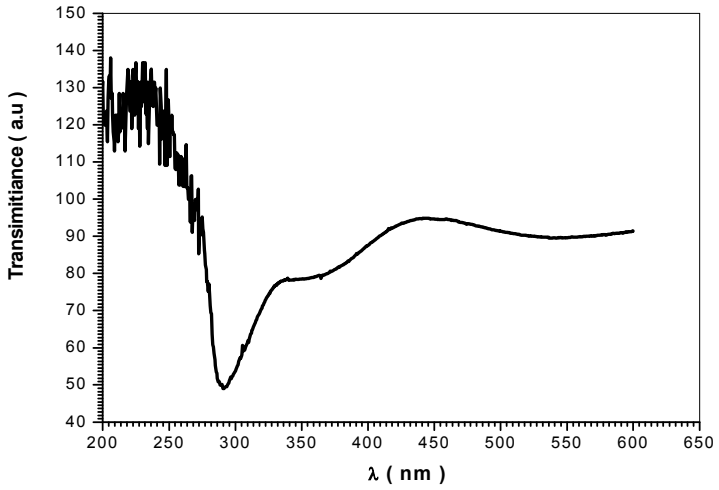

Figure (5.20) shows the relation between transparent and wavelength of ZnO + CuO.

Fig (5.21) shows the optical energy gap (Eg) value of ZnO + CuO thin films. The value of (Eg) obtained was 2. 9 eV.

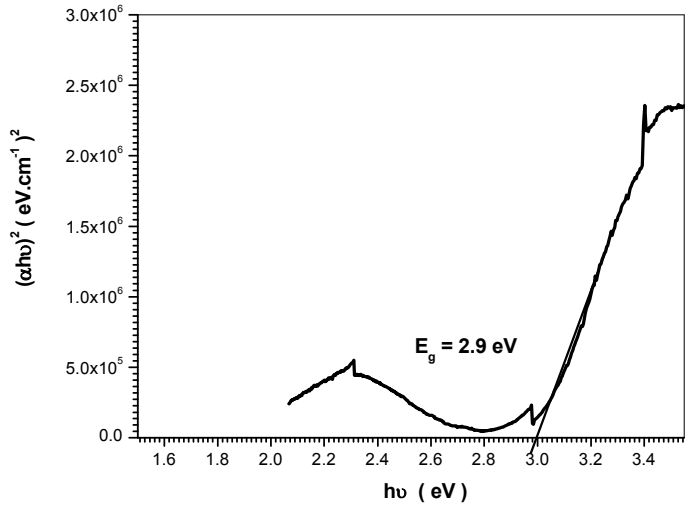

Figure (5.21) the optical energy gap (Eg) value of ZnO + CuO thin films.

Typical I-V curve of ZnO + CuO solar cell for Al electrode as shown in Fig (5.22). It was explain many parameters for cell (Isc), (Voc), (Imax) and (Vmax).

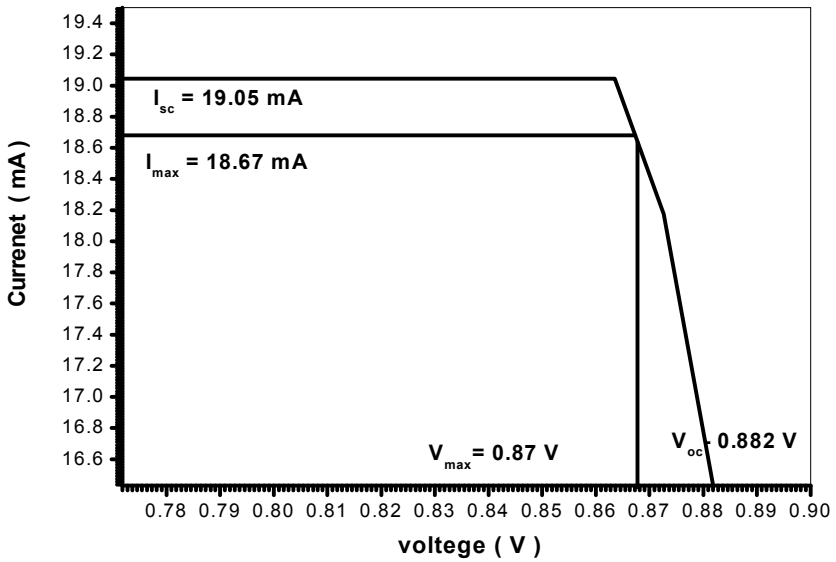

Figure (5.22) Typical I-V curve of the cell of ZnO + CuO thin films for Al electrode.

Table (5.10) Typical I-V riding of the cell of ZnO + CuO thin films for Al electrode.

Voltage (V)	Current (mA)
0.78111	**20.20091**
0.7994	**20.20091**
0.8177	**20.20091**
0.82685	**20.20091**
0.836	**20.20091**
0.84515	**20.20091**
0.8726	**20.20091**
0.88175	**19.33135**
0.89089	**17.59222**

From fig (5.23) it clear show that when was changed the electrode from Al to Ag electrode the parameters value increase.

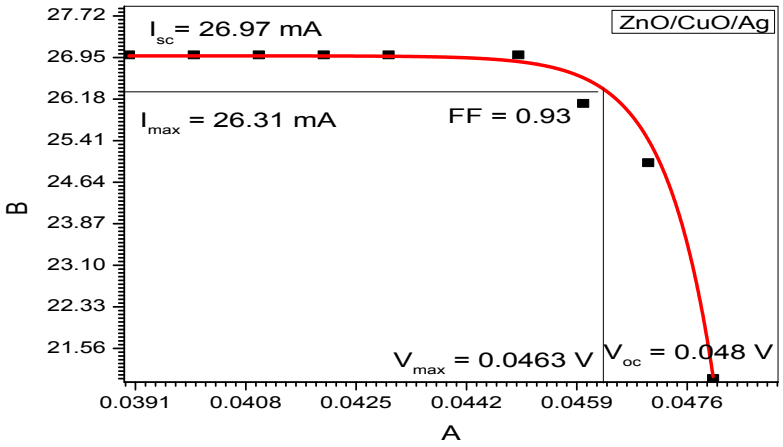

Figure (5.23) Typical I-V curve of the cell of ZnO + CuO thin films for Ag electrode.

Table (5.11) Typical I-V riding of the cell of ZnO + CuO thin films for Ag electrode.

Voltage (V)	Current (mA)
0.039	**27**
0.04	**27**
0.041	**27**
0.042	**27**
0.043	**27**
0.045	**27**
0.046	**26.1**
0.047	**25**
0.048	**21**

From fig (5.24) it clear show that when was changed the electrode from Al to Au electrode the parameters value increase.

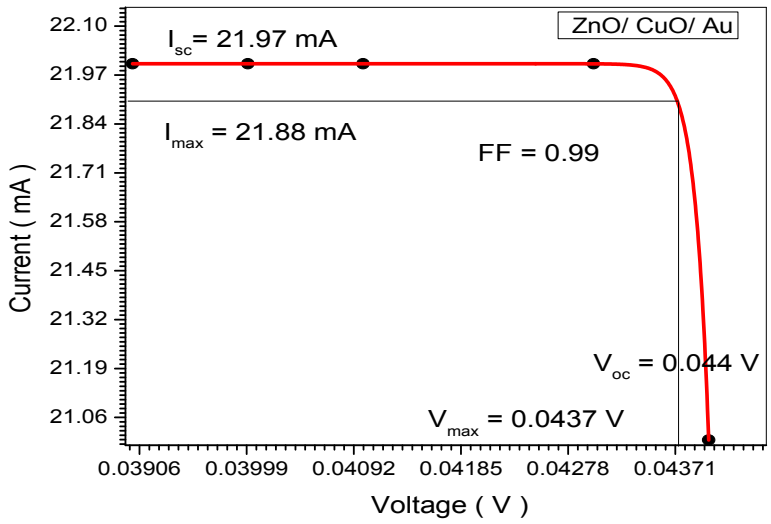

Figure (5.24) Typical I-V curve of the cell of ZnO + CuO thin films for Au electrode.

Table (5.12) Typical I-V riding of the cell of ZnO + CuO thin films for Au electrode.

Voltage (V)	Current (mA)
0.044	**21**
0.043	**22**
0.041	**22**
0.04	**22**
0.039	**22**

Fig (5.25) shows the relation between absorbance and wavelength of DDTTC + MEH-PPV. The rapid increase of the absorption in the low wavelength and sudden increase in special wavelength, this is refer to electronic transition, and this increase is continuous with the increase of photon energy. The range of absorption beak wavelengths for DDTTC + MEH-PPV was obtained at300 nm and 500 nm respectively.

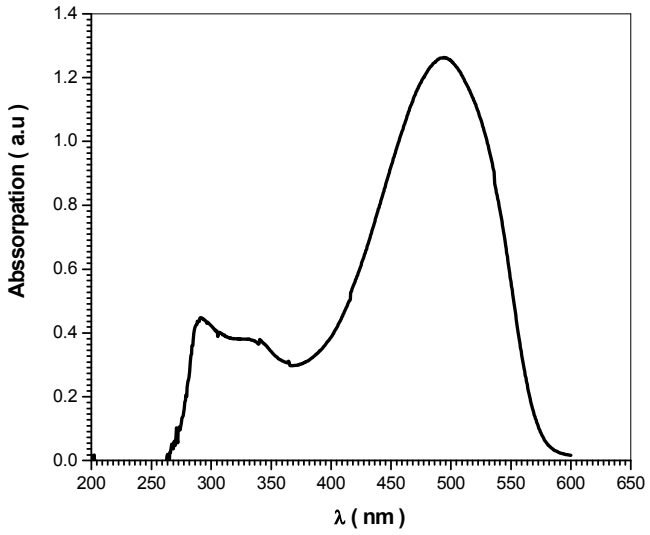

Figure (5.25) shows the relation between absorbance and wavelength of DDTTC + MEH-PPV.

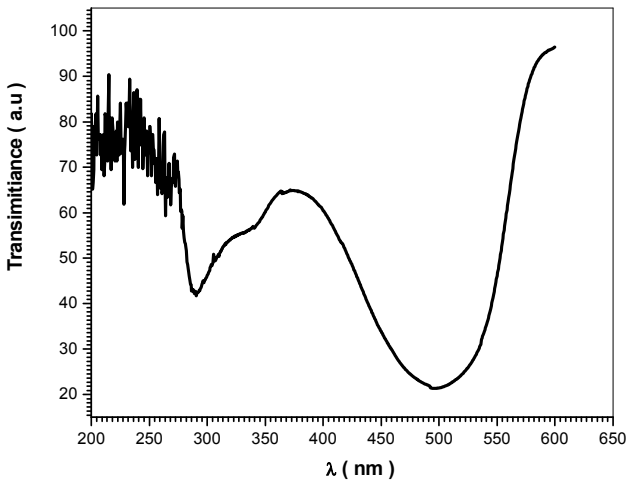

Figure (5.26) shows the relation between transparent and wavelength of DDTTC + MEH-PPV.

Fig (5.27) shows the optical energy gap (Eg) value of DDTTC + MEH-PPV thin films. The value of (Eg) obtained was 2. 2 eV

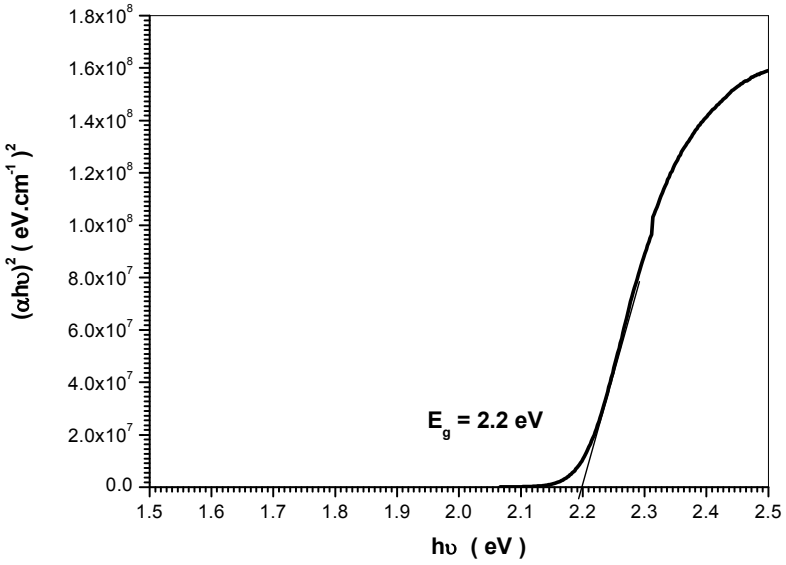

Figure (5.27) the optical energy gap (Eg) value of DDTTC + MEH-PPV thin films.

Typical I-V curve of DDTTC + MEH-PPV solar cell for Al electrode as shown in Fig (5.28). It was explain many parameters for cell (Isc), (Voc), (Imax) and (Vmax).

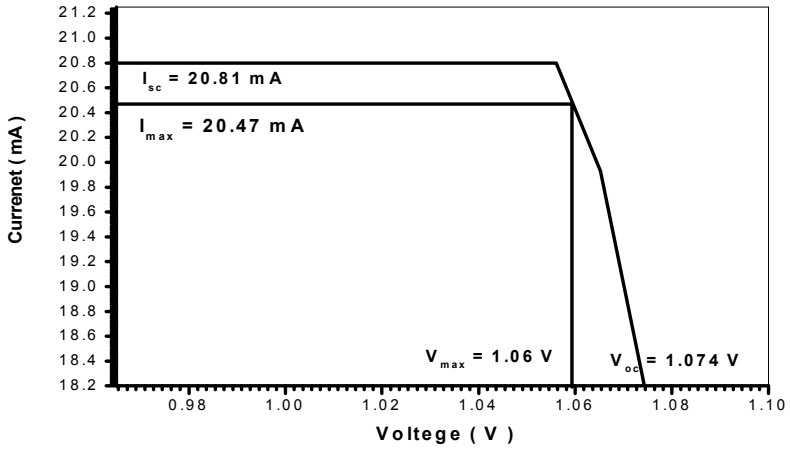

Figure (5.28) Typical I-V curve of the cell of DDTTC + MEH-PPV thin films for Al electrode.

Table (5.13) Typical I-V riding of the cell of DDTTC + MEH-PPV thin films for Al electrode.

Voltage (V)	Current (mA)
0.80761	**20.06841**
0.8259	**20.06841**
0.8442	**20.06841**
0.85335	**20.06841**
0.8625	**20.06841**
0.87165	**20.06841**
0.8991	**20.06841**
0.90825	**19.19885**
0.91739	**17.45972**

From fig (5.29) it clear show that when was changed the electrode from Al to Ag electrode the parameters value increase.

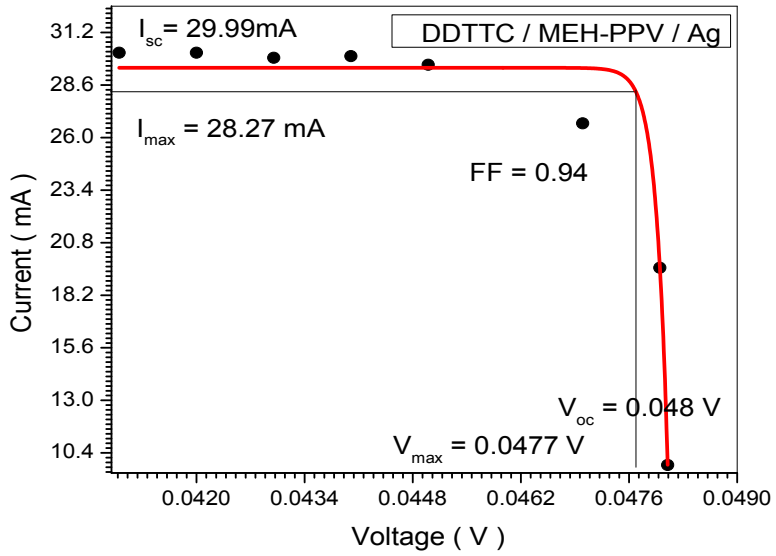

Figure (5.29) Typical I-V curve of the cell of DDTTC + MEH-PPV thin films for Ag electrode.

Table (5.14) Typical I-V riding of the cell of DDTTC + MEH-PPV thin films for Ag electrode.

Voltage (V)	**Current (mA)**
0.041	**30.2**
0.042	**30.2**
0.043	**29.95**
0.044	**30.03**
0.045	**29.6**
0.047	**26.7**
0.048	**19.56**
0.0481	**9.8**

From fig (5.30) it clear show that when was changed the electrode from Al to Au electrode the parameters value increase.

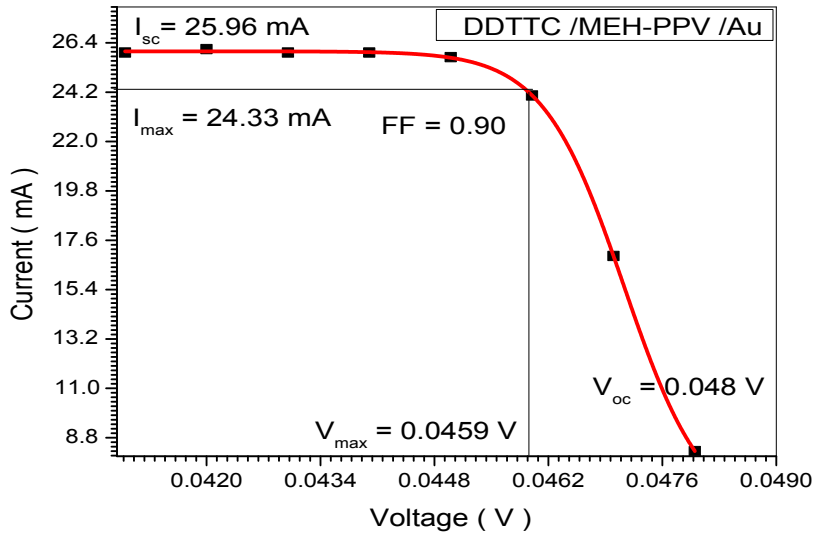

Figure (5.30) Typical I-V curve of the cell of DDTTC + MEH-PPV thin films for Au electrode.

Table (5.15) Typical I-V riding of the cell of DDTTC + MEH-PPV thin films for Au electrode.

Voltage (V)	**Current (mA)**
0.041	**25.97**
0.042	**26.12**
0.043	**25.97**
0.044	**25.97**
0.045	**25.76**
0.046	**24.05**
0.047	**16.9**
0.048	**8.2**

Fig (5.31) shows the relation between absorbance and wavelength of MEH-PPV + DDTTC. The rapid increase of the absorption in the low wavelength and sudden increase in special wavelength, this is refer to electronic transition, and this increase is continuous with the increase of photon energy. The range of absorption beak wavelengths for MEH-PPV + DDTTC was obtained at300 nm and 500 nm respectively.

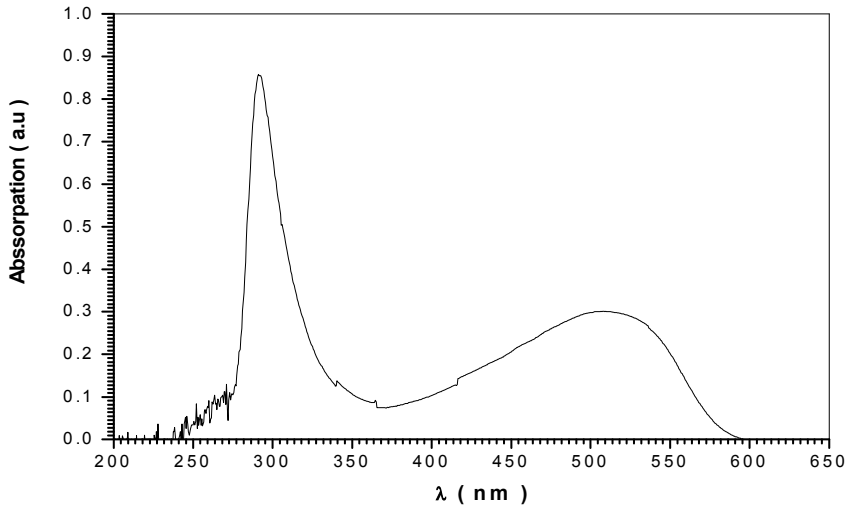

Figure (5.31) shows the relation between absorbance and wavelength of MEH-PPV + DDTTC.

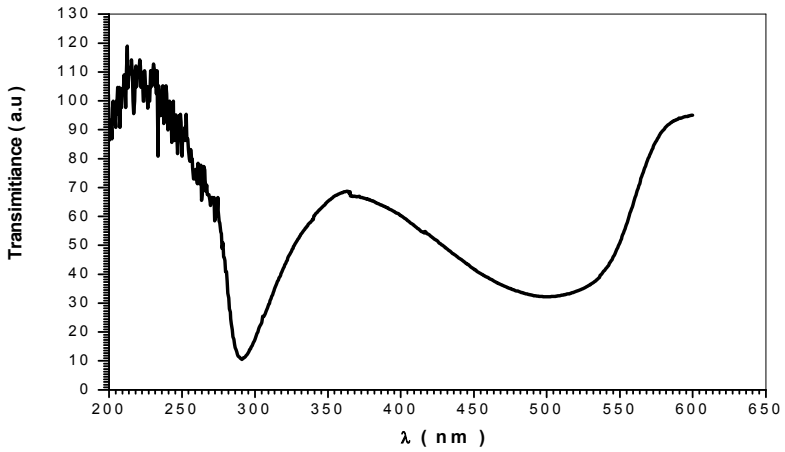

Figure (5.32) shows the relation between transparent and wavelength of MEH-PPV + DDTTC.

Fig (5.33) shows the optical energy gap (Eg) value of MEH-PPV + DDTTC thin films. The value of (Eg) obtained was 2.161 eV.

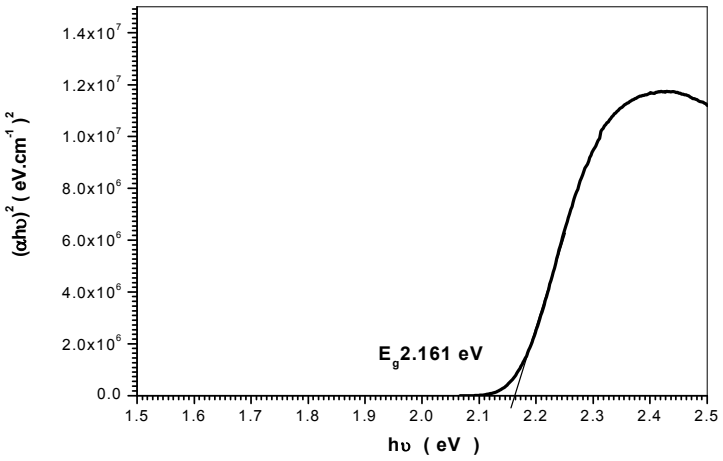

Figure (5.33) the optical energy gap (Eg) value of MEH-PPV + DDTTC thin films.

Typical I-V curve of MEH-PPV + DDTTC solar cell for Al electrode as shown in Fig (5.34). It was explain many parameters for cell (Isc), (Voc), (Imax) and (Vmax).

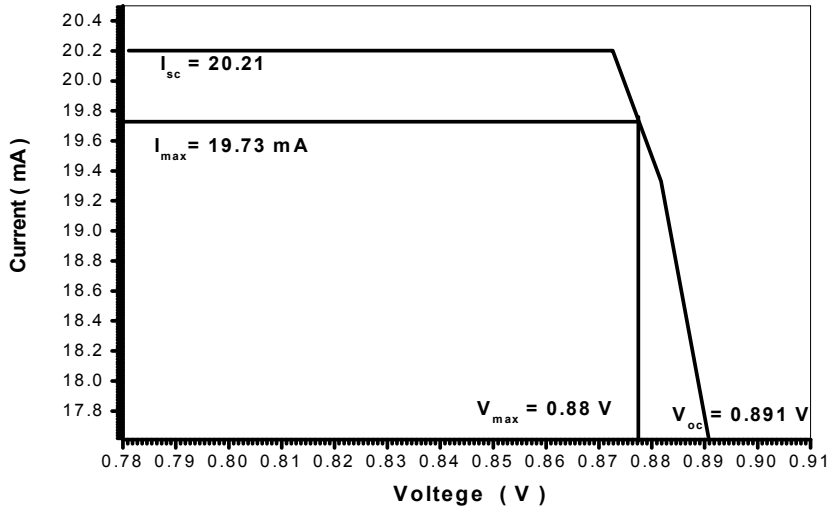

Figure (5.34) Typical I-V curve of the cell of MEH-PPV + DDTTC thin films for Al electrode.

Table (5.16) Typical I-V riding of the cell of MEH-PPV + DDTTC thin films for Al electrode.

Voltage (V)	Current (mA)
0.77201	**19.04341**
0.7903	**19.04341**
0.8086	**19.04341**
0.81775	**19.04341**
0.8269	**19.04341**
0.83605	**19.04341**
0.8635	**19.04341**
0.87265	**18.17385**
0.88179	**16.43472**

From fig (5.35) it clear show that when was changed the electrode from Al to Ag electrode the parameters value increase.

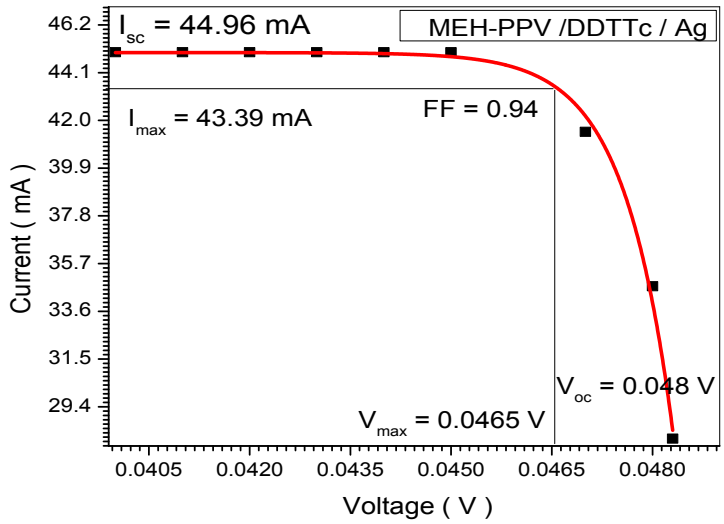

Figure (5.35) Typical I-V curve of the cell of MEH-PPV + DDTTC thin films for Ag electrode.

Table (5.17) Typical I-V riding of the cell of MEH-PPV + DDTTC thin films for Ag electrode.

Voltage (V)	Current (mA)
0.04	**45**
0.041	**45**
0.042	**45**
0.043	**45**
0.044	**45**
0.045	**45**
0.047	**41.5**
0.048	**34.7**
0.0483	**28**

From fig (5.36) it clear show that when was changed the electrode from Al to Au electrode the parameters value increase.

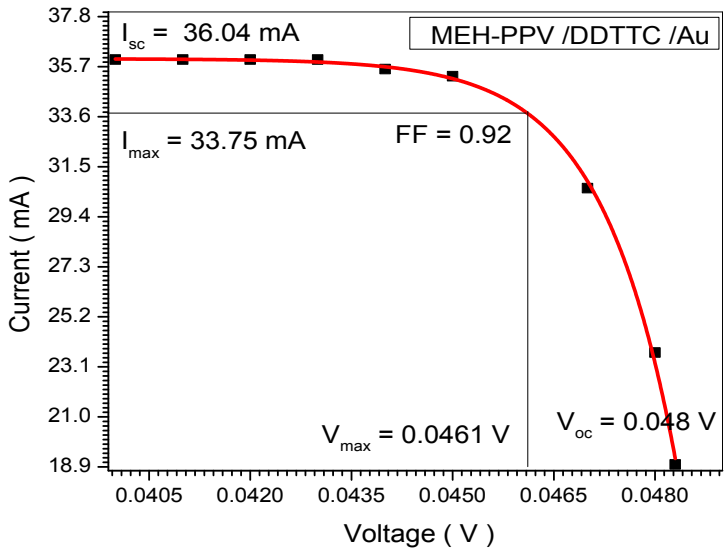

Figure (5.36) Typical I-V curve of the cell of MEH-PPV + DDTTC thin films for Au electrode.

Table (5.18) Typical I-V riding of the cell of MEH-PPV + DDTTC thin films for Au electrode.

Voltage (V)	Current (mA)
0.04	36
0.041	36
0.042	36
0.043	36
0.044	35.6
0.045	35.3
0.047	30.6
0.048	23.7
0.0483	19

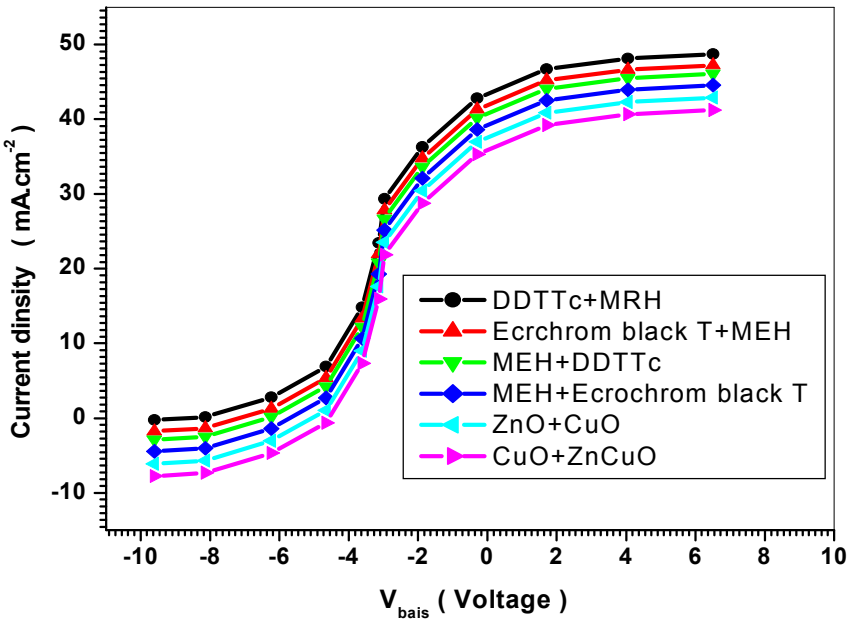

Figure (5.37) Current density as a function of applied voltage for samples used Al electrode.

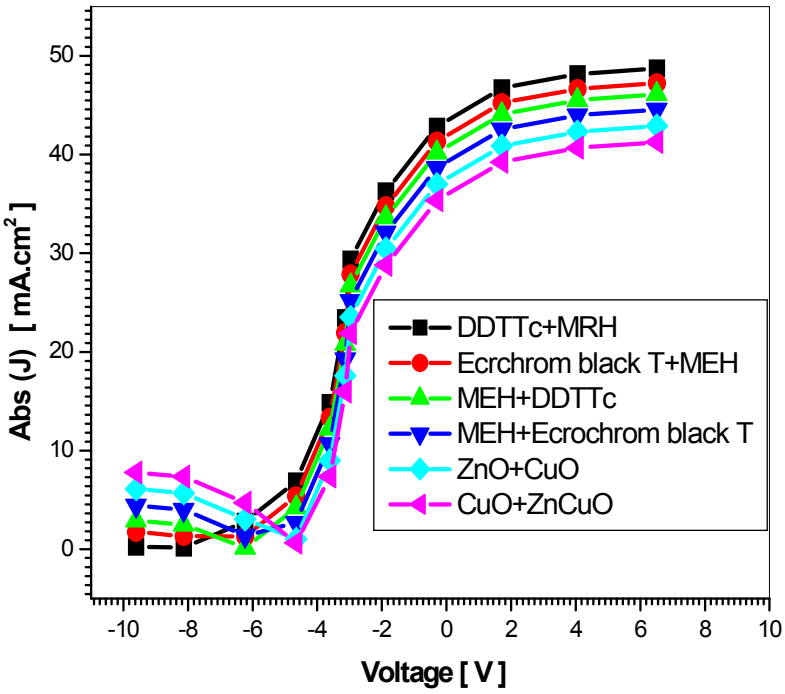

Figure (5.38) the absolute value of the current density as a function of applied voltage at various light intensities for an ITO/ Dyes / MEH-PPV/Al device. Light intensities are approximately 220 mW/cm^2.

Figure (5.39) side view of the layered structure for the ITO/DDTTc /MEH-PPV/Al devices. By AFM image of nanoparticle layer.

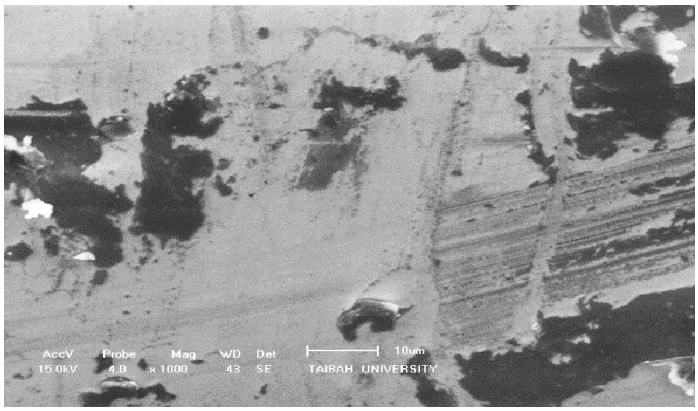

Figure (5.40) side view of the layered structure for the ITO/ Ecrchrom black T /MEH- PPV/Al devices. By AFM image of nanoparticle layer.

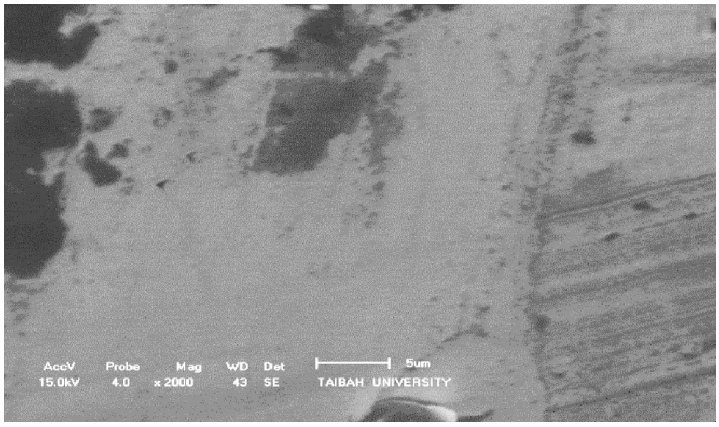

Figure (5.41) side view of the layered structure for the ITO/ZnO+CuO/Al devices. By AFM image of nanoparticle layer.

Figure (5.42) side view of the layered structure for the ITO/CuO+ZnO/Al devices. By AFM image of nanoparticle layer.

Table (5.19) Result of the samples measurement for Al electrode:

Sample	I_{sc}	V_{oc}	I_{max}	V_{max}	J_{sc}	FF	η%
MEH-PPV +Ecrchrom Black T	20.57	0.923	20.16	0.909	3.29	0.965	0.00293
Ecrchrom Black T +MEHPPV	22.18	1.107	21.7	1.09	3.55	0.963	0.00378
CuO +ZnO	20.07	0.918	19.71	0.903	3.21	0.966	0.00284
ZnO + CuO	19.05	0.882	18.67	0.87	3.05	0.966	0.00259
DDTTC+MEH-PPV	20.81	1.074	20.47	1.06	3.33	0.970	0.00347
MEH-PPV+DDTTC	20.21	0.891	19.73	0.88	3.23	0.964	0.00277

Table (5.20) Result of the samples measurement for Ag electrode:

Sample	Isc	Voc	Imax	Vmax	Jsc	FF	η%
MEH-PPV+ Ecrchrom Black T	44.25	0.048	40.78	0.0461	7.080	0.885	0.547
Ecrchrom Black T + MEHPPV	28.99	0.049	27.44	0.0478	4.638	0.923	0.381
CuO +ZnO	25.03	0.048	23.89	0.0466	4.005	0.927	0.324
ZnO + CuO	26.97	0.048	26.31	0.0463	4.315	0.941	0.354
DDTTC+MEH-PPV	29.99	0.048	28.27	0.0477	4.798	0.937	0.392
MEH-PPV+DDTTC	44.96	0.048	43.39	0.0465	7.194	0.935	0.587

Table (5.21) Result of the samples measurement for Au electrode:

Sample	Isc	Voc	Imax	Vmax	Jsc	FF	η%
MEH-PPV+ Ecrchrom Black T	28.99	0.049	27.44	0.0478	4.638	0.923	0.381
Ecrchrom Black T+ MEH-PPV	22.98	0.048	21.78	0.0466	3.677	0.920	0.295
CuO +ZnO	32.03	0.048	30.92	0.0468	5.125	0.941	0.421
ZnO + CuO	21.97	0.044	21.88	0.0437	3.515	0.989	0.278
DDTTC+MEH-PPV	25.96	0.048	24.33	0.0459	4.154	0.896	0.325
MEH-PPV+DDTTC	36.04	0.048	33.75	0.0461	5.766	0.897	0.451

5.2 Discussion

For solar cell devices of the structure (ITO/ Ecrchrom Black T/ MEH-PPV/ Al), Fig (5.37) plots the current density against the applied voltage for these devices on a semi log scale for various light intensities used Al electrode. As one would expect, higher values are seen for both Voc and Jsc for higher incident light intensity. Short-circuit current density (Jsc) is short-circuit current per active area:

$$J_{sc} = I_{sc} \div \text{active aera} \quad \text{mAcm-2}$$

Open circuit voltage (V_{oc}), short circuit current density (Jsc), and the fill factor are measured for samples by examining the J-V curves. The short circuit current density is measured at zero applied bias, while the fill factor is the maximum power delivered to an external load, normalized by the values of Jsc andV_{oc}:

$$\text{Fill factor (ff)} = \frac{(VXJ)_{MAX}}{(V_{OC} \times J_{sc})} \qquad (5.1)$$

Under white light conditions, the energy conversion efficiency (η) is given by

$$\eta = \frac{J_{sc} \times V_{oc} \times FF}{P_{in}} \qquad (5.2)$$

Where $P_{in}$the intensity of incident light, the short circuit current density is depends directly on the external quantum efficiency (the number of carriers collected/number of incident photons).Fill factors, however, decrease for higher light intensities. Improvement in device performance has been observed as devices age. Open circuit voltages and fill factors generally increase as a device ages from a few days to a few months. Table (5.19) shows the result of the samples measurement for Al electrode. The thinner polymer devices have short circuit currents about (20.57 - 22.18) mA for Ecrchrom and (20.07 – 19.05) mA for CuO/ZnO and (20.81 - 20.21) mA for DDTTc, at white-light intensities near 1000 mW.cm-2 used Al electrode. Qualitatively, it is possible to understand why the current density increases with decreasing polymer thickness, conversely to

the fraction of absorbed light. Comparisons of the (DDTTC ‘Eriochrome black T ‘Cu O and ZnO) devices with the thicker MEHPPV device demonstrates that overall the thinner devices have higher fill factors.Fill factors at high light intensity range from (0.965 – 0.963) for the Ecrchrom black T polymer device to (0.966) for CuO ZnO and ZnO CuO device, to (0.97 – 0.964) for the DDTTC polymer device. The lower fill factor for thicker polymer layers is most likely due to higher resistive losses. The quantum efficiencies ranging from a (0.00293 – 0.00378)% peak for the Ecrchrome black T layer, to a (0.00259 – 0.00284)% peak for the CuO/ZnO layer , and to a (0.00347 – 0.00277) % peak for the DDTTC - MEH-PPV layer, consistent with the factor of efficiencies increase seen for the short circuit current densities. The absorption spectra for MEH-PPV is shown in Fig. (5.1), (5.7), (5.25), (5.31) for comparison; the peak device efficiency, located in MEH –PPV, is closely correlated to the peak of (DDTTC ‘Eriochrome black T ‘Cu O and ZnO) for the absorption spectrum. This symbiotic like result is expected for a device where the exciting dissociation occurs at the light incident interface. When the exciting dissociating contact is moved to the opposite side of the device as the incident light, such as for ITO/Al electrode devices, the photo action current spectra can peak at the absorption edge rather than the absorption maximum. Note that these measurements for devices only one day old; as explained above, the device performance improves with age. Hole mobility in MEH-PPV is measured for (DDTTC ‘Eriochrome black T ‘Cu O and ZnO) devices of the type ITO/dye /MEHPPV/ Al by taking J-V curves in the range of 5–50 V and fitting the results to a space-charge limited form for a single carrier Fig(5.37). Since Al does not initially make very good contact to most polymers, these changes are likely due to slow annealing of the Al /polymer interface, creating a better contact and leading to more efficient removal of holes from the device. Such an effect can be partially simulated by thermal annealing of the aluminum electrode once it has been evaporated onto the polymer. Such devices exhibit low dark current densities in forward bias as well as a saturation

of the photocurrent density in forward bias under illumination. The exaction dissociation occurs at the (DDTTC ‘Eriochrome black T ‘Cu O and ZnO) interface, with transfer of the electron to the Al as the important process for charge collection. Moreover, MEH-PPV serves as an effective hole blocker. Our focus in this study is to understand what determines the energy conversion or power Efficiencies in polymer based photovoltaic devices consisting of a (Dyes) layer as the main exaction dissociation site with MEH-PPV as the photoactive polymer semiconductor. Our results consist of measurements where we have modified the different dyes, the different dyes morphology, and the surface roughness of the different dyes layer. Such changes are expected to systematically probe the effects of internal resistance, polymer hole mobility, and surface area of the exaction dissociation site on the charge transport properties of polymer-based photovoltaic. A majority of the charge dissociation occurs at the ITO - polymer interface and the holes must traverse the (DDTTC ‘Eriochrome black T ‘Cu O and ZnO) and the polymer layer to reach the opposite electrode. A type layer of dyes also requires a higher voltage across the device to achieve the same electric field needed to enable exciting dissociation. Type of dyes of the photoactive layer leads to greater absorption and excitant generation, it is generally only the excisions generated within the diffusion length, the electrode-polymer interfaces that are able to contribute to the current density. Other exciting produced deeper with the type of dye before they can exit the device. Once the exciting has been dissociated, one charge is immediately transferred to the close electrode while the remaining one must transverse the (DDTTC ‘Eriochrome black T ‘Cu O and ZnO) to reach the opposite electrode. Because of this layers with correspondingly fewer traps and fewer chances for recombination, allow more current to exit the device. Our results are in agreement with observe a less dramatic effect because the exciting dissociation in our devices is occurring at the transparent electrode and because our (DDTTC ‘Eriochrome black T ‘CuO and ZnO) are well above the exciting diffusion length. In addition, one must take into

account the attenuation of light within the polymer. Due to an attenuation (DDTTC ‘Eriochrome black T ‘CuO and ZnO), only a fraction of the incident light reaches the polymer- Al interface. For other result of samples see table (5.20) and table (5.21) used silver (Ag) and gold (Au) electrodes.

Two different forms of ITO were used to investigate the effects of ITO morphology on the device physics and performance: sintered (DDTTC ‘Eriochrome black T ‘Cu O and ZnO), and anatine ITO nanoparticle layers. Sintered and no sintered (DDTTC ‘Eriochrome black T ‘Cu O and ZnO) layers are both reasonably smooth, with an average surface roughness of 2 nm compared to the nanoparticle layers that can have as much as a 100 nm peak-to-peak roughness, as shown in Fig(5.39) to fig (5.42). We observe higher current densities and more than double the external quantum efficiencies for sintered devices compared to their no sintered counterparts Figs(5.39) and fig (5.40) For example, DDTTC-MEH-PPV sintered device has (0.00347 -0.00277) % peak efficiency while an Eriochrome black T no sintered device has only (0.00293 – 0.00378) % peak efficiency Fig (5.40) Since the morphology of the ITO layers are fairly similar, it is likely that these changes are due to a shift in the ITO Fermi energy level during sintering, leading to more efficient exciting dissociation which is reflected in a slightly higher open circuit voltage. It should be noted, though, that sintering the (DDTTC ‘Eriochrome black T ‘Cu O and ZnO) can sometimes subject the layer to small cracks and therefore to partial shorting which increases the dark current and reduces both the open circuit voltage and the fill factor. Devices made using sintered ITO nanoparticle layers show noticeable improvements in short circuit current density up to (3.33 – 3.23) mA.cm-2, open circuit voltages of (1.074 – 0.891) V, and fill factors of (0.97 – 0.96) at incident light intensity near 1000 mW.cm-2 for DDTTc samples, and other samples see Table (5.19) Quantum efficiency is correspondingly improved, with values as high as (0.00347 – 0.00277) %. These features can likely be explained by

considering the rougher surface of the nanoparticle layer as compared to a (DDTTC ‘Eriochrome black T ‘Cu O and ZnO) layer. The increased surface area of the dissociation interface leads to higher charge extraction from the device and a subsequent decrease in charge recombination.

5.3 CONCLUSIONS

In summary, it clear in this study the photovoltaic properties of solar cells that use an indium titanium oxide layer as a semitransparent anode in conjunction with the photoactive polymer MEH-PPV. It was examined the effect of varying factors such as (DDTTC ‘Eriochrome black T ‘Cu O and ZnO) , polymer mobility, and ITO morphology and have shown that thinner, higher mobility polymer layers combined with rough ITO surfaces lead to the most efficient collection of photo generated carriers. By using large surface area ITO layers as a semitransparent electrode with a polymer and opposing electrode of favorable energy levels, it is able to reduce charge injection and achieve improved fill factors and an order of magnitude increase in External quantum efficiencies. it describe the results using simple models of charge transport in polymer semiconductors where the total current density is a function of the injected current at the metal-polymer interface, the leakage current through the polymer film, and the collected photo generated current that results from the effective dissociation of exciting.

It can very interesting to note that the efficiency of dyes solar cells is higher than that of ZnO/CuO solar cells. This may be attributed to the fact that the dyes have narrow energy gap and large conversion efficiencies. The exchanges of layers also affect for the efficiency. This also related to transparency and conversion efficiencies. The results show change in the efficiency by exchange the electrode from (Al, Ag and Au) and this may due to the atomic size which increases the number of electrons passing to the conduction band.

5.4 Recommendation and Future Work

Due to time constraints, we were not able to accomplish all that we would have wished. We would try to change the CNTs that we are using. First, we would switch to single walled CNTs of varying small diameters (0.8 – 2 nm) to get high absorbance coefficients that match the solar spectrum. These CNTs should also be functionalized to improve their solubility. Ideally, they should be functionalized with the monomer of MEH-PPV-CN to allow them to be fully dissolved and dispersed in the polymer matrix. Good dispersion is key being as we believe our solar cells did not work because CNT agglomerates were shorting the device. Finally, if possible, we would pattern our substrate in such a way that would cause the CNTs to vertically align with the correct spacing to achieve our ideal device structure. Several techniques to vertically align CNTs have been published, but they appear to be beyond the capabilities of the available facilities. Once we have a working device, there are a number of other design considerations that will need to be addressed. They included up scaling the process to make large sheets of cells and packaging issues such as anti-reflective coatings and encapsulation to protect the sensitive organics from the environment. These can largely be accomplished by well understood industrial processes that are currently available. There exist some experiments that still need to be run. The first of which would be to optimize the device thicknesses to get the maximum amount of photon absorption in order to promote excitonic generation. Compartmentalization will also be a key issue with the final device. It will be important to have the cells physically separated so that exposure of one cell to the atmosphere does not jeopardize adjacent cells, and the appropriate size of those individual, discrete cells would need to be determined. It might also be worthwhile to take a closer look at methods for layer generation. While we looked primarily at spin coating, other methods of applying the polymer/CNTs layer

exist, such as atomization and wet processing (e.g. Lanmuir-Blodgett or similar deposition).

Reference

[1] Spanggaad, H.; Krebs, F.C. A brief history of the development of organic and polymeric photovoltaics. Sol. Energ. Mater. Sol. Cells 2004, 83, 125-146.

[2] Coakley, K.; McGehee, M. Conjugated polymer photovoltaic cells. Chem. Mater 2004, 16, 4533-4542.

[3] Simon, J.; André, J-J. Molecular Semiconductors; Springer: Berlin, Germany, 1985.

[4] Pope, M.; Swenberg, C.E. Electronic Processes in Organic Crystals and Polymers; Oxford University Press: New York, NY, USA, 1999.

[5] Savenije, T.J; Warman, J.M; Goosens, A. Visible light sensitisation of titanium dioxide using a phenylene vinylene polymer. Chem. Phys. Lett 1998, 287, 148-153.

[6] Ravirajan, P.; Haque, S.A; Poplavskyy, D.; Durrant, J.R; Bradley, D.D.C; Nelson, J. Nanoporous TiO2 solar cells sensitised with a fullerene-thiophene copolymer. Thin Solid Films 2004, 451-452,624-629.

[7] Ltaief, A.; Davenas, J.; Bouazizi, A.; Ben Chaâbane, R.; Alcouffe, P.; Ben Ouada, H. Film morphology effects on the electrical and optical properties of bulk heterojunction organic solar Cells based on MEH-PPV/C60 composite. Mater. Sci. Engin. C 2005, 25, 67-75.

[8] Ltaief, A.; Bouazizi, A.; Davenas, J.; Alcouffe, P. Influence of the processing conditions on charge transfer and transport properties in poly(2-methoxy-5-(2'-ethylhexyloxy)1-4-phenylenevinylene/C60 composites for photovoltaics. Thin Solid Films 2008, 516, 1578-1583.

[9] Dittmer, J.J.; Marseglia, E.A.; Friend, R.H. Electron trapping in Dye/polymer blend photovoltaic cells. Adv. Mater. 2000, 12, 1270-1274.

[10] Borsenberger PM, Weiss DS (1998) Organic photoreceptors for xerography. Marcel Dekker, New York.

[11] Yersin H (2007) highly efficient OLEDs with phosphorescent materials. Wiley-VCH, Weinheim.

[12] Hertel D, B€assler H (2008) Photoconduction in amorphous organic solids. Chemphyschem 9:666.

[13] Chang EK, Rohlfing M, Louie SG (2000) Excitons and optical properties of alpha-quartz. Phys Rev Lett 85:2613.

[14] All Articles in (2007) Special issue on organic electronics and optoelectronics. Chem Rev 107:923.

[15] Door Waldo J.E. Beek. - Eindhoven, (2005), Hybrid polymer solar cells, TechnischeUniversiteitProefschrift. - ISBN 90-386-2796-3 NUR 913.

[16] KadorL(1991)Stochastic-theory of inhomogeneous spectroscopic line-shapes reinvestigated. J Chem Phys 95:5574.

[17] Coropceanu V, Cornil J, da Silva DA, Olivier Y, Silbey R, Bredas JL (2007) Charge transport in organic semiconductors. Chem Rev 107:926

[18] Warta W, Stehle R, Karl N (1985) Ultrapure, high mobility organic photoconductors. Appl Phys A 36:163.

[19] Schwoerer M, Wolf HC (2007) Organic molecular solids. Wiley-VCH, Weinheim.

[20] Schott M (2006) In: Lanzani G (ed) Photophysics of molecular materials: from single molecules to single crystals. Wiley-VCH, Weinheim, p 49.

[21] Collini E, Scholes RD (2009) Coherent intrachain energy migration in a conjugated polymer at room temperature. Science 323:369.

[22] Barford W, Trembath D (2009) Exciton localization in polymers with static disorder. Phys Rev B 80:165418.

[23] Hoffmann ST, B€assler H, K€ohler A (2010) what determines inhomogeneous broadening of electronic transitions in conjugated polymers. J Phys Chem B 114:17037.

[24] B€assler H (1985) In: Bloor D, Chance RR (eds) Polydiacetylenes. Martinus Nijhof, Dordrecht, the Netherlands, p 135.

[25] Blum T, B€assler H (1988) Reinvestigation of generation and transport of charge-carriers in crystalline polydiacetylenes. Chem Phys 123:431.

[26] Su WP, Schrieffer JR, Heeger AJ (1979) Solitons in polyacetylene. Phys Rev Lett 42:1698 22. Heeger AJ, Kivelson S, Schrieffer JR, Su WP (1988) Solitons in conducting polymers. Rev Mod Phys 60:781.

[27] Arkhipov VI, Fishchuk II, Kadashchuk A, B€assler H (2007) In: Hadziioannou G, Malliaras GG (eds) Semiconducting polymers: chemistry, physics, engineering, vol 1. Wiley-VCH, Weinheim.

[28] Rerum Naturalium, geboren am (1980) Charge Transport In Organic Crystals, Friedrich-Schiller. universitai Jena,seit 1558.p31.

[29] M. Granstro¨m, K. Petritsch, A. C. Arias, A. Lux, M. R. Anderson, and R. H. Friend, Nature –London(395, 257 -1998); A. C. Ariaset al., Phys. Rev. B 60, 1854 -1999.

30. B. O'Regan and M. Gratzel, Nature - London (353, 737 -1991).

[31] For a discussion of the effects of water and oxygen on polymer based photovoltaics, see N. Chawdhury, A. Kohler, M. G. Harrison,D. H. Hang, and R. H. Friend, Synth. Met. 102, 871-1999.

[32] L. Bozano, S. A. Carter, J. C. Scott, G. G. Malliaras, and P. J.Brock, Appl. Phys. Lett. 74, 1132 -1999.

[33] A. C. Arango, L. Johnson, H. Horhold, Z. Schlesinger, and S. A.Carter, Adv. Mater. 12, 1689 -2000.

[34] Doped PEDT is Baytron P, provided by Bayer Corporation. Fordetails, see S. A. Carter, J. C. Scott, and P. J. Brock, Appl. Phys.Lett. 71, 1145 -1997.

[35] The optical power output over the solar spectrum is determined using a calibrated silicon photodetector. Due to uncertainties inreflections and alignment, we estimate an error of 620% for this.

[36] AdnenLtaief1,*, AbdelazizBouazizi1 and Joel Davenas2(Charge Transport in Carbon Nanotubes Polymer Composite Photovoltaic Cells calibration.)Materials 2009, 2,710-718; doi:10.3390/ma2030710 -ISSN 1996-1944www.mdpi.com/journal/materials.

[37] Richard Elkins, Nathan Fierro, Erin Flanagan, Adam Haughton, Michael Kasser, Matthew Stair, and Scott Wilson (Utilizing Carbon Nanotubes to Improve Efficiency of Organic Solar Cells)October 2001 • NREL/CP-520-31019.

[38] Liu Xiao-Dong (刘晓东), Performance improvement of MEH-PPV: PCBM solar cells using bathocuproine and bathophenanthroline as the buffer layers - Chin. Phys. BVol. 20, No. 6 (2011) 068801.

[39] J.H. Parka - Non-linear I–V characteristics of MEH-PPV patterned on sub-micrometer electrodes - Thin Solid Films 393 Ž2001. 129–131.

[40] Mubarak Dirar Abdalla*1, Gasmallah Hassan Hassab Allah2, Mohammed Saeed Daw Elbeit3 & Sawsan Ahmed Elhouri Ahmed4, The Change of Energy Gap and Efficiency of Carbon Solar Cell When Doped by Some Elements, global journal of engineering science and researches,[December2017]ISSN2348 – 8034 DOI- 10.5281/zenodo.1098317 Impact Factor- 4.022.

[41] Asim Ahmed Mohamed Fadol, Determination of Energy Gaps and Effect of Temperature on the Absorption and Transmittance Spectrum on Photoelectrodye, ISSN 2319-5991 www.ijerst.com Vol. 4, No. 3, August 2015 © 2015 IJERST. All Rights Reserved.

[42] Elharam Ali Eltahir Mohammed*1, Mubarak Dirar Abdallah2, Sawsan Ahmed Elhouri Ahmed3 & Rawia A.Elgani4 , Optical Properties of Glass and Plastic Doped by CU, global journal of engineering science and researches ,June 2017] ISSN 2348 – 8034 DOI- 10.5281/zenodo.808172 Impact Factor- 4.022 .

[43] Tayiser MohiEldin Elmahdi, Optical and Electrical Characteristics of TIO2 – MEH Multilayers Thin Film , global journal of engineering science and researches - July 2017 ISSN 2348 – 8034 DOI- 10.5281/zenodo.833354 Impact Factor- 4.022.

[44] Enam Izeldin Ibrahim Elsayd , Energy Gaps, Donor and Accepter Levels for Polymer Solar Cells Doped with Different Dyes, International Journal of Advance Industrial Engineering E-ISSN 2320 –5539 ©2015 INPRESSCO®, All Rights Reserved Available at http://inpressco.com/category/ijaie/ .

[45] Dong-Joo Kwak*, Byung-Ho Moon*, Don-Kyu Lee**, Cha-Soo Park*** and Youl-Moon Sung† - Comparison of Transparent Conductive Indium Tin oxide, Titanium-doped Indium oxide, and Fluorine-doped Tin oxide Films for Dye-sensitized Solar Cell Application - Journal of Electrical Engineering & Technology Vol. 6, No. 5, pp. 684-687, 2011 http://dx.doi.org/10.5370/JEET.2011.6.5.684 .

[46] 1Sakina Ibrahim Ali , 2Mubarak Dirar Abdallah, 3Sawsan Ahmed Elhouri Ahmed - International Journal of Current Trends in Engineering & Research (IJCTER) e-ISSN 2455–1392 Volume 2 Issue 7, July 2016 pp. 82 – 89 Scientific Journal Impact Factor : 3.468 http://www.ijcter.com .

[47] Sakina Ibrahim Ali*, Mubarak Dirar Abdallah, Sawsan Ahmed Elhouri Ahmed, Rawia Abdalgani, Amel Abdalla A, Abdalsakhi. S. M. H - The Relationship between Energy Gab & Efficiency in Dye Solar Cells - International Journal of Engineering Sciences & Research Technology - August, 2016] ISSN: 2277-9655 IC™ Value: 3.00 Impact Factor: 4.116 .

[48] W. Y. Ching and Yong-Nian Xu - PHYSICAL REVIEW B VOLUME 54, NUMBER 19 15 NOVEMBER 1996-I.

[49] Ziad Y. Banyamin 1,*, Peter J. Kelly 1, Glen West 1 and Jeffery Boardman 2 - Electrical and Optical Properties of Fluorine Doped Tin Oxide Thin Films Prepared by Magnetron Sputtering- Coatings 2014, 4,732-746;doi:10.3390/coatings4040732-ISSN20796412
www.mdpi.com/journal/coatings .

[50] Omer Abdalla Omer Gassim, The Effect of Different Dyes on the Efficiency of Polymer Solar Cell, International Journal of Renewable Energy Technology Research; Vol. 3, No. 9, November 2014, pp. 1 - 9, ISSN: 2325 - 3924 (Online) ; Available online at http://ijretr.org.

[51] Thowra Abd Elradi Daldowm, The Effect of Exchanging the ZnO and CnO Layers on Their Performance, International Journal of Advance Industrial Engineering ©2015 INPRESSCO®, All Rights Reserved-E-ISSN2320–5539Available

at http://inpressco.com/category/ijaie/.

[52] Elharam Ali Eltahir Mohammed, Optical Properties of Glass and Plastic Doped by CU, global journal of engineering science and researches, [Mohammed, 4(6): June 2017] ISSN 2348 – 8034, DOI-10.5281/zenodo.808172, Impact Factor- 4.022

[53] Tayiser MohiEldin Elmahdi, Optical and Electrical Characteristics of TIO2 – MEH Multilayers Thin Film, global journal of engineering science and researches, Elmahdi, 4(7): July 2017]ISSN 2348 – 8034, DOI-10.5281/zenodo.833354, Impact Factor-4.022.

[54] Abdelsakhi .S.M - Using Gum Arabic in Making Solar Cells by Thin Films Instead Of Polymers - IOSR Journal of Applied Physics (IOSR-JAP) ISSN: 2278-4861.Volume 8, Issue 1 Ver. III (Jan. - Feb. 2016), PP 27-32 .

[55] James A. Marusek - Solar Storm Threat Analysis - Impact, 2007 James A. Marusek.

[56] Sonya Calnan -Applications of Oxide Coatings in Photovoltaic Devices - Coatings 2014, 4, 162-202; doi:10.3390/coatings4010162/ ISSN 2079-6412 www.mdpi.com/journal/coatings .

[57] Tao C, Ruan S P, Xie G H, Kong X Z, Shen L, Meng F X, Liu C X, Zhang X D, Dong W and Chen W Y 2009 Appl. Phys. Lett. 94 043311.

[58] A. Bewick, M. Fleischmann, H.R. Thirsk, Trans. Faraday Soc., 58 (1962) 2200.

[59] Sariciftci NS (1997) Primary photoexcitations in conjugated polymers: molecular exciton versus semiconductor band model. Word Scientific, Singapore.

[60] I. Danaee, F. Shoghi, M. DehghaniMobarake, M. Kameli, J. Solid State Electrochem. 14 (2010) 57.

[61] S. Bijani, R. Schrebler, E.A. Dalchiele, M. Gabás, L. Martínez, and J. R. Ramos-Barrado, J. Phys. Chem. C, 115 (2011) 21373.

[62] T.L. Barr, Y.L. Liu, J. Phys. Chem. Solids, 50 (1989) 657.

[63] B.D. Cullity, Elements of X-ray Diffraction 2nd Ed. (Addi-son-Wesley, Reading, MA, 1978).

[64] W. Vallejo, J. Clavijo, Brazilian Journal of Physics, 40 (2010) 30.

[65] P. O'Brien, D. J. Otway, and J. R.Walsh, Thin Solid Films, 315 (1998) 57.

[66] Friend RH, Gymer RW, Holmes AB, Burroughes JH, Marks RN, Taliani C, Bradley DDC, Dos Santos DA, Bredas JL, Logdlund M, Salaneck WR (1999) Electroluminescence in conjugated polymers. Nature 397:121.

[67] Klingshirn CF. Zinc Oxide from fundamental properties towards novelapplications. Heidelberg; London: Springer; 2010.

[68] Xu S, Wang ZL. One-dimensional ZnO nanostructures: Solution growth and functional properties. Nano Research. 2011; 4:1013-98.

[69] Jagadish C, Pearton SJ. Zinc oxide bulk, thin films and nanostructures processing, properties and applications. Amsterdam; London: Elsevier; 2006.